Finite element simulation of the thermoviscoplastic behaviour of bituminous concrete

P. Royis and J.F. Seignol *

August 31, 2022

Abstract

The general framework of the paper deals with the finite element modelling of thermomechanical problems involving viscous materials. The study focuses on the statement of constitutive equations describing the thermoviscoplastic behaviour of bituminous concrete, as well as on their implementation in a finite element program. After stating the general equations of the space- and time-continuous problem and the constitutive relations governing the viscoplastic component of the bituminous concrete behaviour, we deal with their integration over finite time steps, considering two different schemes. Eventually, two sets of numerical results are presented. The first one, an homogeneous triaxial test, is used to compare those schemes, whereas the second one consists of numerical simulations of real-size experiments performed on a road structure subjected to thermal and mechanical loadings. By comparing the numerical results with experimental ones, it allows us to test the finite element code on a more complex and realistic problem.

1 Introduction

The general framework of this paper deals with the finite element modelling of thermomechanical problems involving viscous materials such as bituminous concrete. The need for precise predictions in civil engineering leads to more and more complex constitutive equations of geomaterials used in finite element programs. In the particular case of bituminous concrete, widely used in road construction and other structures, a realistic model must take into account the thermoviscoplastic component of its behaviour, if one wants to lay out the corresponding structures correctly.[1,2,3,4,5,6] The use of viscoplastic constitutive equations for describing the non-linear and rate-sensitive behaviour of other geomaterials, such as clays, is now well established and many rheological models have been issued from this formalism.[7,8,9] The study described in this paper focuses on the statement of constitutive equations describing the thermoviscoplastic behaviour of bituminous concrete, as well as on their implementation in the finite element program ELFIMTH developed in previous works for the numerical resolution of boundary value problems in thermomechanics.[10,11,12,13]

*Ecole Nationale des Travaux Publics de l'Etat, DGCB URA CNRS 1652, 69518 Vaulx-en-Velin Cedex, France

The paper consists of three main sections. In each of them, except in subsection 4.1, the sign conventions of the continuum mechanics will be used for stresses and strains. We shall then consider that stresses are positive in traction and negative in compression. Consequently, positive strains represent extensions, whereas negative strains represent contractions. The first main section is devoted to the statement of the time-continuous thermomechanical problem. The frame of the study is restricted to small perturbations (i.e. small strains and small displacements) and quasistatic transformations of the materially simple continua considered, and we assume that the influence of thermodynamical coupling effects on the temperature field are very weak. The most important part of that first section deals with the description of the tensorial constitutive relations governing the viscoplastic component of the bituminous concrete behaviour, which are put up on the basis of experimental results obtained by Di Benedetto[2,5] and Yan[4,5] at the LGM (Laboratoire GéoMatériaux) of the ENTPE (Ecole Nationale des Travaux Publics de l'Etat, France). More precisely, the statement of those constitutive equations is based on the geometrical shape of a viscoplastic criterion proposed by Di Benedetto[5] from experimental data obtained by Yan[4] on cylindrical samples of bituminous concrete, combined with one-dimensional relations[2,5] giving the breaking axial stresses for axisymmetric triaxial tests in compression on cylindrical samples of bituminous concrete, with constant lateral stress and constant axial strain rate.

The second section focuses on the weak formulation od the time-discretized thermomechanical problem. Taking into account the previous assumption relating to thermodynamical coupling effects, this problem is divided into a thermal one and a mechanical one, with unilateral coupling. The most important part of that second section is devoted to the time discretization of the viscoplastic component of the constitutive equations considered. And indeed, the main difficulty when using such equations for finite element computations lies in their integration over finite time steps. For that purpose robust time-discrete schemes are needed if one wants to obtain accurate numerical approximations at a reasonable cost. The term 'robust' means here that those schemes remain stable for sufficiently large values of the time step. More generally speaking, the bringing into play of robust schemes is advisable as soon as unelastic constitutive laws are considered. That subject has been studied intensively as regards both rate-dependent and rate-independent equations.[14,15,16,17] For instance, it is well known that explicit integration formulae showing good stability properties when used for rate-independent constitutive laws[14,15] can turn out to be excessively expensive for rate-dependent ones whenever their stability regions become too small. A first way of avoiding this drawback consists in using semi- or fully implicit schemes which bring unconditional stability.[16] This leads to solve iteratively a non-linear system of equations as soon as non-linear constitutive relations are considered. Another approach using semi-implicit Runge-Kutta methods has been suggested by Rosenbrock[18] in order to increase stability while avoiding fully implicit schemes. Halfway between explicit and implicit methods are also the forward gradient schemes, which have been successfully implemented in finite element codes when combined with efficient time-stepping strategies.[17] But both Rosenbrock and forward gradient procedures are not, in general, unconditionally stable. Although the viscoplastic constitutive relations considered in the paper are non-linear, the framework of the first approach is chosen. Two different schemes are used for the time discretization of those constitutive equations: the classical θ-scheme and an original method, developed in previous works[19,20] for linear and non-linear viscoelastic models, based on a direct integration of the constitutive equations over finite time steps. The resulting time-discretized mechanical problems become non-linear when another scheme than the θ-scheme with $\theta = 0$ is used. Since in this case rheological non-linearities can increase greatly, their iterative resolution

is carried out by using the robust Newton method.

Eventually, the third section presents two sets of numerical examples. The first one, consisting of simulations of homogeneous triaxial tests, is used to compare the different time-discrete schemes. The second one is the simulation of real-size experiments performed on a road structure at the LAVOC (LAboratoire des Voies de Circulation) of the EPFL (Ecole Polytechnique Fédérale de Lausanne, Switzerland). By comparing the numerical results with experimental ones, it allows us to test the finite element program on a problem with thermal and mechanical loadings.

2 The time-continuous thermomechanical problem

2.1 General considerations

Let Ω be a materially simple continuum, the motion of which is studied over the time-interval $[0, \mathrm{T}]$. We shall denote as Γ the boundary of Ω, and as $\mathbf{n}$ the outer unit normal to Γ. Ω is assumed to be an open, bounded and simply connected region of $\mathbb{R}^3$, and its boundary Γ is assumed to be lipschitz-continuous. The successive configurations of this continuum will be observed with respect to the same fixed orthonormal frame, and we shall assume small strains and small displacements. Eventually we consider only quasistatic problems, for which the acceleration may be ignored, and we assume that the influence of thermodynamical coupling effects on the temperature field are very weak. The problem stated in the two following subsections 2.2 and 2.3 consists then in determining both histories $T(t,.)$ and $\mathbf{u}(t,.)$ of the temperature and displacement fields of the continuum Ω, over the time-interval $[0, \mathrm{T}]$.

2.2 The space and time-continuous thermal problem

Let $T(t,.)$ be the absolute temperature field of the continuum Ω at the time t and let $\mathbf{q}(t,.)$ be the vectorial field of heat flux at the same time. We denote as ρ the mass density, as c_T the heat capacity at constant volume, as λ_T the thermal conductivity of the material, and as $Q(t,.)$ the field of internal heat generation per unit volume in Ω at time t. We assume that c_T and λ_T are functions of the absolute temperature T.

On the other hand, we denote as $\Gamma_1(t)$ the part of Γ on which the temperature is imposed at time t (Dirichlet boundary conditions), as $\Gamma_2(t)$ the part of Γ on which the values of the heat flux per unit area are prescribed at time t (Neumann boundary conditions), and as $\Gamma_3(t)$ the part of Γ on which the heat flux per unit area is governed, at the same time, by the convective surface heat transfer with the ambient medium (Fourier boundary conditions). We assume that $\Gamma_1(t)$, $\Gamma_2(t)$ and $\Gamma_3(t)$ constitute, at every time t, a partition of Γ such that $\Gamma_1(t)$ has at least one point, and we denote as $T_i(t,.)$ the values of the temperature imposed on $\Gamma_1(t)$, as $\varphi(t)$ the values of the heat flux per unit area given on $\Gamma_2(t)$, as h_T the convective surface heat transfer coefficient, and as T_a the temperature of the ambient medium. The convective coefficient h_T is a function of the temperature on $\Gamma_3(t)$.

As mentioned in the previous subsection 2.1, we consider only quasistatic problems, for which the acceleration may be ignored, and we assume that the influence of thermodynamical coupling effects on the temperature field are very weak. So the problem which consists in determining the

history $T(t,.)$ of the temperature of Ω over the time-interval $[0, \mathrm{T}]$ is governed by the following set of equations:

$$\left\{\begin{array}{rrcll} (1.1) & \mathrm{div}_x\mathbf{q}(t,x) & = & Q(t,x) - \rho c_T \dot{T}(t,x) & \left.\begin{array}{l}\\\end{array}\right\} \text{in }]0,\mathrm{T}[\times\Omega \\ (1.2) & \mathbf{q}(t,x) & = & -\lambda_T \mathbf{grad}_x T(t,x) & \\ (1.3a) & T(t,x) & = & T_i(t,x) & \text{on }]0,\mathrm{T}[\times\Gamma_1(t) \\ (1.3b) & \mathbf{q}(t,x).\mathbf{n} & = & \varphi(t,x) & \text{on }]0,\mathrm{T}[\times\Gamma_2(t) \\ (1.3c) & \mathbf{q}(t,x).\mathbf{n} & = & h_T\left(T(t,x) - T_a\right) & \text{on }]0,\mathrm{T}[\times\Gamma_3(t) \\ (1.4) & T(0,x) & = & T_0(x) & \text{in } \Omega \end{array}\right. \tag{1}$$

The equation (1.1) arises from the application of the energy balance for conduction dominated heat flow in an elementary volume $\mathrm{d}\Omega$ subject to thermal, elastic and viscoplastic training, when the influence of thermodynamical coupling effects on the temperature field are very weak. The equation (1.2) is the Fourier heat conduction law. The boundary conditions are given by equations (1.3a), (1.3b) and (1.3c). Finally, equation (1.4) provides initial conditions of the problem.

2.3 The space and time-continuous mechanical problem

Let $\mathbf{b}(t,.)$ be the vectorial field at time t of the body forces acting per unit volume on Ω. We shall denote as $\Gamma_4(t)$ the part of Γ on which we have, at time t, the essential boundary conditions $\mathbf{u}\,|\Gamma_4(t) = \mathbf{u}_i$, where $\mathbf{u}_i(t,.)$ is the field of the displacements given on $\Gamma_4(t)$, and as $\Gamma_5(t)$ the part of Γ on which the values of the stress vector are prescribed at the same time. We assume that $\Gamma_4(t)$ and $\Gamma_5(t)$ constitute, at every time t, a partition of Γ such that $\Gamma_4(t)$ has at least three points, and we denote as $\mathbf{g}(t,.)$ the values of the stress vector given on $\Gamma_5(t)$.

Let now $\varepsilon(t,.)$ be the linearized tensorial field of the small strains in Ω at time t, and let $\sigma(t,.)$ be the tensorial field of the Cauchy stresses in Ω at the same time. This paper focuses on the finite element modelling of geomaterials, such as bituminous concrete, the behaviour of which is described by a thermoviscoplastic constitutive law. For that we assume an additive decomposition of the total strain rate tensor $\dot{\varepsilon}$ into linear elastic, viscoplastic and thermal components, as follows:

$$\dot{\varepsilon} = \dot{\varepsilon}^{(e)} + \dot{\varepsilon}^{(vp)} + \dot{\varepsilon}^{(th)} \tag{2}$$

The linear elastic part is given by

$$\dot{\varepsilon}^{(e)} = \mathbf{C} : \dot{\sigma} \tag{3}$$

where $\mathbf{C}$ is the classical fourth-order tensor of elastic compliances. The viscoplastic component is controlled by the following constitutive relation

$$\dot{\varepsilon}^{(vp)} = \mathbf{F}(\sigma, T) \tag{4}$$

involving the absolute temperature T. The expression of the tensorial function $\mathbf{F}$, which generalizes the one-dimensional relations obtained by Di Benedetto[2,5] from experimental results of axisymmetric triaxial tests, will be described in the following subsection 2.4. The third term on the right-hand side in equation (2), corresponding to the thermal strains, is given by

$$\dot{\varepsilon}^{(th)} = \alpha(T)\dot{T}\mathbf{I}_2 \tag{5}$$

where $\dot{T}$ is the rate of temperature, $\alpha(T)$ the coefficient of thermal expansion, which is a function of the absolute temperature T, and where $\mathbf{I}_2$ denotes the second-order unit tensor.

Then the problem which consits in determining the history $\mathbf{u}(t,.)$ of the displacements of Ω over the time interval $[0,\mathrm{T}]$ is governed by the following set of equations:

$$\left\{\begin{array}{lrcll}
(6.1a) & \mathbf{div}_x\sigma(t,x) & = & -\mathbf{b}(t,x) & \\
(6.1b) & \sigma^{\mathrm{T}}(t,x) & = & \sigma(t,x) & \\
(6.2) & \dot{\varepsilon}(t,x) & = & \mathbf{C}:\dot{\sigma}(t,x)+\mathbf{F}\left(\sigma(t,x),T(t,x)\right) & \\
 & & + & \alpha\left(T(t,x)\right)\dot{T}(t,x)\mathbf{I}_2 & \\
(6.3a) & \mathbf{u}(t,x) & = & \mathbf{u}_i(t,x) \quad \text{on }]0,\mathrm{T}[\times\Gamma_4(t) & \\
(6.3b) & \sigma(t,x).\mathbf{n} & = & \mathbf{g}(t,x) \quad \text{on }]0,\mathrm{T}[\times\Gamma_5(t) & \\
(6.4a) & \mathbf{u}(0,x) & = & \mathbf{u}_0(x) & \\
(6.4b) & \sigma(0,x) & = & \sigma_0(x) & \\
(6.4c) & \varepsilon(0,x) & = & 0 &
\end{array}\right.
\begin{array}{l}
\left.\begin{array}{l}\\ \\ \\ \end{array}\right\}\ \text{in }]0,\mathrm{T}[\times\Omega \\
\left.\begin{array}{l}\\ \\ \\ \end{array}\right\}\ \text{in } \Omega
\end{array} \qquad (6)$$

Equations (6.1a) and (6.1b) arise from the application of the balance principle of linear and angular momentum, in the absence of body and surface couples. Equation (6.2) is the formulation of the constitutive law of the viscoplastic materially simple continuum Ω, under the assumption of small transformations. The boundary conditions are given by equations (6.3a) and (6.3b). Finally, relations (6.4a), (6.4b) and (6.4c) provide initial conditions of the problem.

In the following subsection 2.4 we give the detailed expression of the viscoplastic component (4) of the strain rate tensor.

2.4 Description of the viscoplastic component of the strain rate tensor

The viscoplastic criterion, proposed by Di Benedetto[5] from experimental data obtained by Yan[4] on cylindrical samples of bituminous concrete, is defined, in the orthonormal space $\mathbb{R}^3$ of principal stresses, by two cone-shaped parts with apex on the trisector $\sigma_1=\sigma_2=\sigma_3$. The intersections of both of these conic parts with the deviatoric planes (i.e. the planes which are orthogonal to the trisector) are equilateral triangles, the vertices of which are located on the projections (onto these planes) of the negative half-axes of $\mathbb{R}^3$. The figure 1 shows the geometrical shape of that criterion in the bisecting plane $\sigma_2=\sigma_3$ (fig. 1.a), as well as in the deviatoric plane common to both of its parts (fig. 1.b).

This criterion is isotropic and convex. Its interior defines the states of stresses for which the viscoplastic component of the strain rate is inactive ($\dot{\varepsilon}^{(vp)}=0$), and for which the behaviour of the continuum is assumed to be linear elastic. The states of stresses exterior to the criterion and located in deviatoric planes intersecting it are those for which the viscoplastic component is active. The other states of stresses, located in deviatoric planes which have no intersection with the criterion, are assumed to be not allowed. They are defined by $\mathrm{tr}\sigma \geq 3\sigma_{0t}$, where the point with coordinates $\sigma_1=\sigma_2=\sigma_3=\sigma_{0t}$ is the apex of the criterion (fig. 1).

In addition to the geometrical shape of the viscoplastic criterion shown on figure 1 we have also the following expression (Di Benedetto[2,5]) of the breaking axial stresses $\sigma_1^{(c)}$, for axisymmetric triaxial tests in compression ($\sigma_1\leq\sigma_2=\sigma_3$) on cylindrical samples of bituminous concrete with constant lateral stress $\sigma_2=\sigma_3$ and constant axial strain rate $\dot{\varepsilon}_1<0$. Let us remind the reader that the sign conventions are those used in continuum mechanics (i.e. the tensile

stresses are positive and the compressive ones are negative, and that consequently positive strains represent extensions whereas negative strains represent contractions).

$$\left\{ \begin{array}{l} \dfrac{-\sigma_1^{(c)}}{\sigma_u} = \alpha \dfrac{-\sigma_3}{\sigma_u} + \beta(T, c_p) \ln \left(\dfrac{-\dot{\varepsilon}_1 + \delta(T)}{\dot{\varepsilon}_u} \right) + \gamma(T, c_p) \\ \text{with } \alpha = \alpha_c \text{ if } \sigma_3 \leq 0 \text{ and } \alpha = \alpha_t \text{ if } \sigma_3 \in]0, \sigma_{0t}] \end{array} \right. \tag{7}$$

In this expression α_c and α_t are two positive given constants such that $\alpha_t > \alpha_c > 1$, β and γ are two given functions of the absolute temperature T and of the compactness c_p, and δ is a given function of the absolute temperature. As to the constants σ_u and $\dot{\varepsilon}_u$, they are units of stress and strain rate, respectively.

For the same axisymmetric triaxial tests in compression, we get also [5] the residual axial stresses after relaxation $\sigma_1^{(cr)}$ by setting $\dot{\varepsilon}_1 = 0$ in the previous expression (7):

$$\left\{ \begin{array}{l} \dfrac{-\sigma_1^{(cr)}}{\sigma_u} = \alpha \dfrac{-\sigma_3}{\sigma_u} + \beta(T, c_p) \ln \left(\dfrac{\delta(T)}{\dot{\varepsilon}_u} \right) + \gamma(T, c_p) \\ \text{with } \alpha = \alpha_c \text{ if } \sigma_3 \leq 0 \text{ and } \alpha = \alpha_t \text{ if } \sigma_3 \in]0, \sigma_{0t}] \end{array} \right. \tag{8}$$

These residual stresses are also given by the above criterion (Di Benedetto[5]) when restricted to the half-plane $\sigma_1 \leq \sigma_2 = \sigma_3$. In particular we have, by setting $\sigma_1^{(cr)} = \sigma_3 = \sigma_{0t}$ in expression (8), the following relation binding σ_{0t}, α_t, T and c_p:

$$(1 - \alpha_t)\sigma_{0t} + \sigma_u \beta(T, c_p) \ln \frac{\delta(T)}{\dot{\varepsilon}_u} + \sigma_u \gamma(T, c_p) = 0 \tag{9}$$

For given $\dot{\varepsilon}_1 < 0$, T and c_p, relations (7) and (8) show that the breaking stresses $\sigma_1^{(c)}$ for axisymmetric triaxial tests in compression are located on two straight lines parallel to the criterion. The experimental data obtained by Yan[4] corroborate this feature for the tests in extension. More precisely, for given $c > 0$, T and c_p, the breaking axial stresses $\sigma_a^{(c)}$ in compression (resp. $\sigma_a^{(t)}$ in extension) for axisymmetric triaxial tests with constant lateral stress σ_l and constant axial strain rate $\dot{\varepsilon}_a = -c$ (resp. $\dot{\varepsilon}_a = c$) can be obtained from the above criterion by similarity, as shown by the figure 2. Moreover, this criterion gives the residual stresses after relaxation $\sigma_a^{(cr)}$ (resp. $\sigma_a^{(tr)}$).

Eventually, the viscoplastic flow rule is assumed to be axisymmetric cone-shaped round the trisector in the orthonormal space $\mathbb{R}^3$ of principal stresses, and the principal directions of the viscoplatic component $\dot{\varepsilon}^{(vp)}$ of the strain rate tensor are assumed to be identical with those of the Cauchy stress tensor σ. Therefore the direction $\mathbf{d}_{\dot{\varepsilon}^{(vp)}}$ of $\dot{\varepsilon}^{(vp)}$, which is defined by $\mathbf{d}_{\dot{\varepsilon}^{(vp)}} = \dot{\varepsilon}^{(vp)} / \|\dot{\varepsilon}^{(vp)}\|$ where $\|\dot{\varepsilon}^{(vp)}\| = \sqrt{\dot{\varepsilon}_{ij}^{(vp)} \dot{\varepsilon}_{ij}^{(vp)}})$ is the Euclidian norm of $\dot{\varepsilon}^{(vp)}$, is entirely defined, from the above axisymmetric triaxial tests in compression, by the tangent Poisson ratio at viscoplastic flow ν_∞, which may be assumed to be independent of the axial strain rate $\dot{\varepsilon}_a < 0$ and of the temperature T when considering the experimental data obtained by Yan.[4]

On the basis of the previous considerations coming from experimental works we shall now develop the tensorial expression of the viscoplastic component $\dot{\varepsilon}^{(vp)} = \mathbf{F}(\sigma, T)$ of the strain rate tensor. To begin with, let us denote as $\mathbf{s}$ the deviatoric part of the stress tensor σ, defined by $\mathbf{s} = \sigma - \sigma_m \mathbf{I}_2$ with $3\sigma_m = \mathrm{tr}\sigma$. We assume that the state of stress σ is such that the viscoplastic

component of the strain rate tensor is active ($\dot{\varepsilon}^{(vp)} \neq 0$). Then the above assumptions relating to the viscoplastic flow rule and the principal directions of $\dot{\varepsilon}^{(vp)}$ lead to the following expression of $\mathbf{d}_{\dot{\varepsilon}^{(vp)}}$:

$$\mathbf{d}_{\dot{\varepsilon}^{(vp)}} = A_1 \mathbf{I}_2 + A_2 \frac{\mathbf{s}}{\|\mathbf{s}\|} \tag{10}$$

where A_1 and A_2 are two constants to be determined. But, for axisymmetric triaxial tests in compression with constant lateral stress $\sigma_2 = \sigma_3$ and constant axial strain rate $\dot{\varepsilon}_1 < 0$, we have the following expression of $\dot{\varepsilon}^{(vp)}$ and $\mathbf{s}$ at viscoplastic flow:

$$\dot{\varepsilon}^{(vp)} = \dot{\varepsilon}_1 \begin{pmatrix} 1 & 0 & 0 \\ 0 & -\nu_\infty & 0 \\ 0 & 0 & -\nu_\infty \end{pmatrix} \qquad \mathbf{s} = \frac{\sigma_1^{(c)} - \sigma_3}{3} \begin{pmatrix} 2 & 0 & 0 \\ 0 & -1 & 0 \\ 0 & 0 & -1 \end{pmatrix} \tag{11}$$

We then get

$$\mathbf{d}_{\dot{\varepsilon}^{(vp)}} = \frac{-1}{\sqrt{1+2\nu_\infty^2}} \begin{pmatrix} 1 & 0 & 0 \\ 0 & -\nu_\infty & 0 \\ 0 & 0 & -\nu_\infty \end{pmatrix} \qquad \frac{\mathbf{s}}{\|\mathbf{s}\|} = \frac{-1}{\sqrt{6}} \begin{pmatrix} 2 & 0 & 0 \\ 0 & -1 & 0 \\ 0 & 0 & -1 \end{pmatrix} \tag{12}$$

which gives

$$\mathbf{d}_{\dot{\varepsilon}^{(vp)}} = -\frac{1}{3} \frac{1-2\nu_\infty}{\sqrt{1+2\nu_\infty^2}} \mathbf{I}_2 + \sqrt{\frac{2}{3}} \frac{1+\nu_\infty}{\sqrt{1+2\nu_\infty^2}} \frac{\mathbf{s}}{\|\mathbf{s}\|} \tag{13}$$

Therefore, taking into account the uniqueness of the decomposition of a second-order symmetric tensor into isotropic and deviatoric parts, we obtain the following expressions of the constants A_1 and A_2:

$$A_1 = -\frac{1}{3} \frac{1-2\nu_\infty}{\sqrt{1+2\nu_\infty^2}} \qquad A_2 = \sqrt{\frac{2}{3}} \frac{1+\nu_\infty}{\sqrt{1+2\nu_\infty^2}} \tag{14}$$

In other words the expression (13) of $\mathbf{d}_{\dot{\varepsilon}^{(vp)}}$ holds, not only for axisymmetric triaxial tests in compression, but also for any given state of stress σ for which the viscoplastic component $\dot{\varepsilon}^{(vp)}$ is active. Now there remains for us to give the general expression of the norm $\|\dot{\varepsilon}^{(vp)}\|$ of that component.

For that purpose let σ_1, σ_2 and σ_3 be the principal values of σ, and let M be the point with coordinates $(\sigma_1, \sigma_2, \sigma_3)$ in the orthonormal space $\mathbb{R}^3$ of principal stresses. Then M belongs to a unique surface obtained by similarity from the viscoplastic criterion, as shown on figure 2. This surface is entirely determined by the scalar D defined on the same figure. The expression of D as a function of the principal stresses is given by

$$D = \sqrt{\frac{3}{2}} \max\{s_1, s_2, s_3\} = \sqrt{\frac{3}{2}} \left(\max\{\sigma_1, \sigma_2, \sigma_3\} - \sigma_m \right) \tag{15}$$

where s_1, s_2 and s_3 are the eigenvalues of $\mathbf{s}$. Note that the set of points (x_1, x_2, x_3) of $\mathbb{R}^3$ such that $\max\{x_1, x_2, x_3\} - (x_1 + x_2 + x_3)/3 = \sqrt{2/3}D$ is the cylinder, parallel to the trisector, the section of which is the equilateral triangle obtained by intersection of the previous surface with the deviatoric plane (Π) containing the point $M(\sigma_1, \sigma_2, \sigma_3)$ (fig. 2).
As mentioned above, the surface obtained by similarity from the viscoplastic criterion as shown on figure 2 and to which M belongs can also be got, for a given $c > 0$, by axisymmetric triaxial tests in compression and in extension with constant lateral stress $\sigma_l \leq \sigma_{0t}$ and constant axial

strain rate $\dot{\varepsilon}_a = \pm c$. For the tests in compression ($\dot{\varepsilon}_a = -c < 0$) the breaking axial stresses $\sigma_a^{(c)}$ and the residual axial stresses after relaxation $\sigma_a^{(cr)}$ are then given by the relations (7) and (8), respectively. By substracting equation (8) from (7) we obtain the following expression:

$$\frac{-\sigma_a^{(c)} + \sigma_a^{(cr)}}{\sigma_u} = \beta(T, c_p) \ln\left(1 + \frac{c}{\delta(T)}\right) \tag{16}$$

which is obviously independent of σ_l and of the function $\gamma(T, c_p)$. For $\sigma_l = 0$ and taking into account the notations in figure 2, we have $\sigma_a^{(c)} = -\sigma_0^{(c)}$ and $\sigma_a^{(cr)} = -\sigma_0^{(cr)}$, respectively. So, from the previous equation (16) we obtain the following expression of c:

$$c = \delta(T)\left(\exp\left(\frac{1}{\beta(T, c_p)} \frac{\sigma_0^{(c)} - \sigma_0^{(cr)}}{\sigma_u}\right) - 1\right) \tag{17}$$

From equation (8) and for $\sigma_l = 0$ we have also

$$\frac{\sigma_0^{(cr)}}{\sigma_u} = \beta(T, c_p) \ln \frac{\delta(T)}{\dot{\varepsilon}_u} + \gamma(T, c_p) \tag{18}$$

So relation (17) can be replaced by the following one:

$$c = \dot{\varepsilon}_u \exp\left(\frac{1}{\beta(T, c_p)}\left(\frac{\sigma_0^{(c)}}{\sigma_u} - \gamma(T, c_p)\right)\right) - \delta(T) \tag{19}$$

On the other hand, by considering the figure 2, we have the following relation binding the scalars D and $\sigma_0^{(c)}$:

$$\begin{cases} 2D = \sqrt{\dfrac{2}{3}}\sigma_0^{(c)} + \dfrac{1}{\sqrt{3}}\left(-\mathrm{tr}\sigma - \sigma_0^{(c)}\right)\tan\left(\theta - \theta_0\right) \\ \text{with } \theta = \theta_c \text{ if } \mathrm{tr}\sigma \leq -\sigma_0^{(c)} \text{ and } \theta = \theta_t \text{ if not} \end{cases} \tag{20}$$

By reconsidering the same figure 2, for any given state of stress σ for which the viscoplastic component $\dot{\varepsilon}^{(vp)}$ is active and taking into account the expression (15) of D, we have $\mathrm{tr}\sigma \leq -\sigma_0^{(c)} \iff D \leq -1/\sqrt{6}\mathrm{tr}\sigma \iff \max\{\sigma_1, \sigma_2, \sigma_3\} \leq 0$. Moreover the following equalities hold:

$$\begin{cases} \tan\theta_0 = \dfrac{1}{\sqrt{2}} \\ \tan\theta_c = \dfrac{\alpha_c}{\sqrt{2}} \\ \tan\theta_t = \dfrac{\alpha_t}{\sqrt{2}} \end{cases} \tag{21}$$

Thus we have

$$\begin{cases} \tan\left(\theta - \theta_0\right) = \sqrt{2}\dfrac{\alpha - 1}{\alpha + 2} \\ \text{with } \alpha = \alpha_c \text{ if } \max\{\sigma_1, \sigma_2, \sigma_3\} \leq 0 \text{ and } \alpha = \alpha_t \text{ if not} \end{cases} \tag{22}$$

and the previous relation (20) gives

$$\begin{cases} \sigma_0^{(c)} = \dfrac{(2 + \alpha)\sqrt{6}D + (\alpha - 1)\,\mathrm{tr}\sigma}{3} \\ \text{with } \alpha = \alpha_c \text{ if } \max\{\sigma_1, \sigma_2, \sigma_3\} \leq 0 \text{ and } \alpha = \alpha_t \text{ if not} \end{cases} \tag{23}$$

or, taking into account the expression (15) of D

$$\left\{\begin{array}{l}\sigma_0^{(c)} = -\mathrm{tr}\sigma \ + (2+\alpha)\max\{\sigma_1,\sigma_2,\sigma_3\} \\ \text{with } \alpha = \alpha_c \text{ if } \max\{\sigma_1,\sigma_2,\sigma_3\} \leq 0 \text{ and } \alpha = \alpha_t \text{ if not}\end{array}\right. \tag{24}$$

Then the expression (19) which defines the surface containing M (see figure 2) becomes

$$\left\{\begin{array}{l} c = \dot{\varepsilon}_u \exp\left(\dfrac{1}{\beta(T,c_p)}\left(\dfrac{-\mathrm{tr}\sigma \ + (2+\alpha)\max\{\sigma_1,\sigma_2,\sigma_3\}}{\sigma_u} - \gamma(T,c_p)\right)\right) - \delta(T) \\ \text{with } \alpha = \alpha_c \text{ if } \max\{\sigma_1,\sigma_2,\sigma_3\} \leq 0 \text{ and } \alpha = \alpha_t \text{ if not}\end{array}\right. \tag{25}$$

Unfortunately, althoug this expression of c holds for any given state of stress σ for which the viscoplastic component $\dot{\varepsilon}^{(vp)}$ is active, it is not sufficient to give the corresponding expression of $\|\dot{\varepsilon}^{(vp)}\|$. However, for axisymmetric triaxial tests in compression with constant lateral stress $\sigma_2 = \sigma_3$ and constant axial strain rate $\dot{\varepsilon}_1 = -c < 0$, the expression (11) of $\dot{\varepsilon}^{(vp)}$ gives immediately

$$\|\dot{\varepsilon}^{(vp)}\| = c\sqrt{1+2\nu_\infty^2} \tag{26}$$

As to the axisymmetric triaxial tests in extension with constant lateral stress $\sigma_2 = \sigma_3$ and constant axial strain rate $\dot{\varepsilon}_1 = c > 0$, the expression (13) of $\mathbf{d}_{\dot{\varepsilon}^{(vp)}}$ leads to

$$\|\dot{\varepsilon}^{(vp)}\| = 3c\frac{\sqrt{1+2\nu_\infty^2}}{1+4\nu_\infty} \tag{27}$$

So, owing to the isotropy of the viscoplastic criterion and of the surface containing M and obtained from this criterion by similarity as shown on figure 2, we suggest to express $\|\dot{\varepsilon}^{(vp)}\|$ by using the following interpolation

$$\left\{\begin{array}{l}\|\dot{\varepsilon}^{(vp)}\| = c\left(\dfrac{N_t+N_c}{2} + \dfrac{N_t-N_c}{2}\cos(3\phi)\right) \\ \text{with } N_c = \sqrt{1+2\nu_\infty^2} \text{ and } N_t = 3\dfrac{\sqrt{1+2\nu_\infty^2}}{1+4\nu_\infty}\end{array}\right. \tag{28}$$

where the Lode angle ϕ is defined on figure 2. The value of $\cos(3\phi)$ is given by

$$\cos(3\phi) = 3\sqrt{6}\frac{s_1 s_2 s_3}{\|\mathbf{s}\|^3} = \sqrt{6}\mathrm{tr}(\mathbf{d}_\mathbf{s}^3) \tag{29}$$

In that expression $\mathbf{d_s}$ denotes the direction of $\mathbf{s}$ defined by $\mathbf{d_s} = \mathbf{s}/\|\mathbf{s}\|$, where $\|\mathbf{s}\| = \sqrt{s^{ij}s^{ij}}$ is the Euclidian norm of $\mathbf{s}$.

Thus relations (25) and (28) give the general expression of $\|\dot{\varepsilon}^{(vp)}\|$ which leads to the general form of the viscoplastic component $\dot{\varepsilon}^{(vp)}$, taking into account the expression of $\mathbf{d}_{\dot{\varepsilon}^{(vp)}}$ given by equation (13). Let us remind the reader that this component is inactive if the point M with coordinates $(\sigma_1,\sigma_2,\sigma_3)$ is located inside the viscoplastic criterion, and that the states of stresses located in deviatoric planes which have no intersection with this criterion are not allowed. In the first case we have $\sigma_0^{(c)} \leq \sigma_0^{(cr)}$ and in the second one $\mathrm{tr}\sigma \geq 3\sigma_{0t}$, where σ_{0t} is defined on figure 1. By considering equations (9) and (18), we have also the following expression of σ_{0t}:

$$\sigma_{0t} = \frac{\sigma_0^{(cr)}}{\alpha_t - 1} \tag{30}$$

Finally, from all the above considerations, we can give the general expression of $\dot{\varepsilon}^{(vp)}$.

$$\dot{\varepsilon}^{(vp)} = \mathbf{F}(\sigma, T) = \phi_1(\sigma, T)\left[C_1 - C_2 \mathrm{tr}(\mathbf{d}_\mathbf{s}^3)\right]\left[\phi_2(\sigma, T) - \delta(T)\right]\left[-C_3\mathbf{I}_2 + C_4\mathbf{d}_\mathbf{s}\right] \tag{31}$$

with:

$$\left\{\begin{array}{rcl} \phi_1(\sigma,T) & = & Y\left(\sigma_0^{(c)} - \sigma_0^{(cr)}\right) Y\left(-\mathrm{tr}\sigma + \dfrac{3\sigma_0^{(cr)}}{\alpha_t - 1}\right) \\ \phi_2(\sigma,T) & = & \dot{\varepsilon}_u \exp\left(\dfrac{1}{\beta(T,c_p)}\left(\dfrac{\sigma_0^{(c)}}{\sigma_u} - \gamma(T,c_p)\right)\right) \\ \sigma_0^{(cr)} & = & \sigma_u\left(\beta(T,c_p)\ln\dfrac{\delta(T)}{\dot{\varepsilon}_u} + \gamma(T,c_p)\right) \\ \sigma_0^{(c)} & = & -\mathrm{tr}\sigma \ + (2+\alpha)\max\{\sigma_1,\sigma_2,\sigma_3\} \\ C_1 = 2\dfrac{1+\nu_\infty}{1+4\nu_\infty} & & C_2 = \sqrt{6}\dfrac{2\nu_\infty - 1}{1+4\nu_\infty} \quad C_3 = \dfrac{1-2\nu_\infty}{3} \quad C_4 = \sqrt{\dfrac{2}{3}}(1+\nu_\infty) \\ \text{with } \alpha = \alpha_c \text{ if } \max\{\sigma_1,\sigma_2,\sigma_3\} \leq 0 \text{ and } \alpha = \alpha_t \text{ if not} & & \end{array}\right. \tag{32}$$

where Y denotes the Heaviside function.

We shall now focus on the time discretization of the continuous thermomechanical problem described in this section, and then on the weak formulation of the resulting time-discretized problems.

3 Weak formulation of the time-dicretized thermomechanical problem

Let $N \in \mathbb{N}^*$ and let $t_0, t_1, \ldots, t_N$ be an increasing sequence of time values such that $t_0 = 0$ and $t_N = \mathrm{T}$. In the following we are interested in the displacement fields $\mathbf{u}(t_n, .)$ and in the temperature fields $T(t_n, .)$ relating to the time values t_n, $n \in \{1, \ldots, N\}$. We put, $\forall n \in \{0, \ldots, N\}$ and $\forall x \in \Omega$, $\mathbf{u}_n(x) = \mathbf{u}(t_n, x)$, as well as analogous notations for t, T, σ, ε, $\mathbf{b}$, $\mathbf{g}$, Q, $\mathbf{u}_i$, T_i and φ, and we denote as Δt_n the time-increment $t_n - t_{n-1}$, $n \in \{1, \ldots, N\}$. The two following subsections 3.1 and 3.2 are devoted to the weak formulation of the time-discretized thermal and mechanical problems, respectively, whereas the subsection 3.3 focuses on the particularly important point constituted by the time discretization of the constitutive equations (2), (3), (5), (31) and (32).

3.1 Weak formulation of the time-discretized thermal problem

The time discretization of the continuous thermal problem (1) requires to approximate the time derivative $\dot{T}$ of the absolute temperature T. In order to ensure the unconditional stability we choose to make this approximation by using the fully implicit Euler scheme. So we obtain, from (1), the following sequence of time-dicretized problems $(\mathbf{Q}_n)$, $n \in \{1, \ldots, N\}$:

$$(\mathbf{Q}_n)\left\{\begin{array}{lrcll} (33.1) & \mathrm{div}_x\left(\lambda_{T_n}\mathbf{grad}_x T_n(x)\right) + Q_n(x) & = & \rho c_{T_n}\dfrac{T_n(x) - T_{n-1}(x)}{\Delta t_n} & \text{in } \Omega \\ (33.2a) & T_n(x) & = & T_{in}(x) & \text{on } \Gamma_1(t_n) \\ (33.2b) & -\lambda_{T_n}\mathbf{grad}_x T_n(x).\mathbf{n} & = & \varphi_n(x) & \text{on } \Gamma_2(t_n) \\ (33.2c) & -\lambda_{T_n}\mathbf{grad}_x T_n(x).\mathbf{n} & = & h_{T_n}\left(T_n(x) - T_a\right) & \text{on } \Gamma_3(t_n) \end{array}\right. \tag{33}$$

Let now $W = H^1(\Omega)$ be the Sobolev space of real square integrable functions defined on Ω with square integrable first-order generalized derivatives. For any given $n \in \{1, \ldots, N\}$ we denote as W_n the closed subspace of W of the functions $w \in W$ such that $w\,|\Gamma_1(t_n) = 0$. Let us then consider the product of $w \in W_n$ and the equation (33.1) and integrate the resulting expression on Ω. Thus, after integration by parts and use of the Gauss integral identity, and taking into account the boundary conditions (33.2b) and (33.2c), we obtain the classical weak formulation $(\mathbf{Q}_{nv})$ of $(\mathbf{Q}_n)$:

$$(\mathbf{Q}_{nv}) \left\{ \begin{array}{l} \text{Find } T_n \in W \text{ such that} \\ \displaystyle\int_\Omega \left(\frac{\rho c_{T_n}}{\Delta t_n} (T_n - T_{n-1})\, w + \lambda_{T_n} \mathbf{grad}_x T_n . \mathbf{grad}_x w + \right) \mathrm{d}\Omega + \int_{\Gamma_3(t_n)} h_{T_n} (T_n - T_a)\, w \,\mathrm{d}\Gamma \\ \qquad\qquad = \displaystyle\int_\Omega Q_n w \,\mathrm{d}\Omega - \int_{\Gamma_2(t_n)} \varphi_n w \,\mathrm{d}\Gamma \qquad \forall w \in W_n \\ T_n = T_{in} \text{ on } \Gamma_1(t_n) \end{array} \right. \tag{34}$$

The variational problem $(\mathbf{Q}_{nv})$ can then be solved by the finite element method after building a finite element space $W_h \subset W$. The problem $(\mathbf{Q}_{nh})$ coming from the finite element space discretization, like $(\mathbf{Q}_{nv})$, is non linear since c_T, λ_T and h_T are functions of the temperature. However these non linearities remain weak, which allows us to perform the resolution of $(\mathbf{Q}_{nh})$ by using the fixed point method, easy to implement. If $T_n^{(r)}$ is the approximation coming from the resolution of the linearized problem $(\mathbf{Q}_{nh}^{(r)})$ relating to the iteration (r), then $(\mathbf{Q}_{nh}^{(r+1)})$ takes the following form:

$$\left(\mathbf{Q}_{nh}^{(r+1)}\right) \left\{ \begin{array}{l} \text{Find } T_n^{(r+1)} \in W_h \text{ such that } \forall w \in W_h \cap W_n \\ \displaystyle\int_\Omega \left(\frac{\rho c_{T_n^{(r)}}}{\Delta t_n} T_n^{(r+1)} w + \lambda_{T_n^{(r)}} \mathbf{grad}_x T_n^{(r+1)} . \mathbf{grad}_x w + \right) \mathrm{d}\Omega + \int_{\Gamma_3(t_n)} h_{T_n^{(r)}} T_n^{(r+1)} w \,\mathrm{d}\Gamma \\ \qquad\qquad = \displaystyle\int_\Omega \left(\frac{\rho c_{T_n^{(r)}}}{\Delta t_n} T_{n-1} + Q_n \right) w \mathrm{d}\Omega - \int_{\Gamma_2(t_n)} \varphi_n w \,\mathrm{d}\Gamma + \int_{\Gamma_3(t_n)} h_{T_n^{(r)}} T_a w \,\mathrm{d}\Gamma \\ T_n^{(r+1)} = T_{in} \text{ on } \Gamma_1(t_n) \end{array} \right. \tag{35}$$

The stop of iterations is governed by the following test

$$\left| \frac{T_n^{(r+1)} - T_n^{(r)}}{T_n^{(r)}} \right| \leq e^{(tol)} \tag{36}$$

where $e^{(tol)}$ has a sufficient small value, for instance $e^{(tol)} = 10^{-6}$.

Thus, the iterative resolution of $(\mathbf{Q}_{nh})$ gives the approximate value of T_n needful for the resolution of the mechanical problem relating to the time value t_n. This last problem, which is obviously solved after $(\mathbf{Q}_{nh})$, constitutes the matter of the following subsection 3.2.

3.2 Weak formulation of the time-discretized mechanical problem

The developments made in the following subsection 3.3 devoted to the time discretization of the constitutive equations (2), (3), (5), (31) and (32) lead, for given $n \in \{1, \ldots, N\}$ and $x \in \Omega$, to the following formal relation

$$\varepsilon_n(x) = \mathbf{H}_{nx} \left(\sigma_n(x), \mathcal{H}_{nx} \right) \tag{37}$$

where $\mathcal{H}_{nx}$ denotes the set of memory parameters different from $\sigma_n(x)$ at point x and at time t_n, including especially $T_n(x)$, $\varepsilon_{n-1}(x)$ and $\sigma_{n-1}(x)$. The tensorial function $\mathbf{H}_{nx}$, which is non-linear with respect to $\sigma_n(x)$ when another scheme than a fully explicit one is chosen for the time discretization of the constitutive equations, is assumed to be one-to-one, according to the principle of determinism. So we can write, formally

$$\sigma_n(x) = \mathbf{H}_{nx}^{-1}\left(\varepsilon_n(x), \mathcal{H}_{nx}\right) \tag{38}$$

Let now $V = \left(H^1(\Omega)\right)^3$. For any given $n \in \{1, \ldots, N\}$ we denote as V_n the closed subspace of V of the functions $\mathbf{v} \in V$ such that $\mathbf{v}\,|\Gamma_4(t_n) = 0$. Let us then consider the inner product of $\mathbf{v} \in V_n$ and the equation (6.1a) obtained for $t = t_n$ and integrate the resulting expression on Ω. Thus, after integration by parts and use of the Gauss integral identity, and taking into account the previous relation (38) together with the boundary conditions (6.3b) at time t_n, we obtain the classical weak formulation $(\mathbf{P}_{nv})$ of the time-discretized mechanical problem relating to the time value t_n:

$$(\mathbf{P}_{nv}) \left\{ \begin{array}{l} \text{Find } \mathbf{u}_n \in V \text{ such that} \\ \displaystyle\int_\Omega \mathbf{H}_{nx}^{-1}\left(\varepsilon(\mathbf{u}_n), \mathcal{H}_{nx}\right) : \varepsilon(\mathbf{v})\,\mathrm{d}\Omega = \int_\Omega \mathbf{b}_n.\mathbf{v}\,\mathrm{d}\Omega + \int_{\Gamma_5(t_n)} \mathbf{g}_n.\mathbf{v}\,\mathrm{d}\Gamma \qquad \forall \mathbf{v} \in V_n \\ \mathbf{u}_n = \mathbf{u}_{in} \text{ on } \Gamma_4(t_n) \end{array} \right. \tag{39}$$

where the operator ε is defined by $\varepsilon(.) = \left(\mathbf{grad}_x(.) + \mathbf{grad}_x^{\mathbf{T}}(.)\right)/2$.

The space-discrete approximation $(\mathbf{P}_{nh})$ of $(\mathbf{P}_{nv})$ is then obtained after building a finite element space $V_h \subset V$. As mentioned above $(\mathbf{P}_{nh})$, like $(\mathbf{P}_{nv})$, is non-linear when another scheme than a fully explicit one is used for the time discretization of the constitutive equations. Since in this last case the rheological non-linearities can increase greatly, the iterative resolution of $(\mathbf{P}_{nh})$ is carried out by using the robust Newton method. If $\mathbf{u}_n^{(r)}$ is the approximation coming from the resolution of the linearized problem $(\mathbf{P}_{nh}^{(r)})$ relating to the iteration (r), then $(\mathbf{P}_{nh}^{(r+1)})$ takes the following form:

$$(\mathbf{P}_{nh}^{(r+1)}) \left\{ \begin{array}{l} \text{Find } \mathbf{u}_n^{(r+1)} \in V_h \text{ such that } \forall \mathbf{v} \in V_h \cap V_n \\ \displaystyle\int_\Omega \varepsilon(\mathbf{v}) : \mathbf{G}_{nx}^{-1}\left(\sigma_n^{(r)}, \mathcal{H}_{nx}\right) : \varepsilon(\mathbf{u}_n^{(r+1)})\,\mathrm{d}\Omega = \int_{\Gamma_5(t_n)} \mathbf{g}_n.\mathbf{v}\,\mathrm{d}\Gamma \\ \qquad\qquad + \displaystyle\int_\Omega \left(\varepsilon(\mathbf{v}) : \left(\mathbf{G}_{nx}^{-1}\left(\sigma_n^{(r)}, \mathcal{H}_{nx}\right) : \mathbf{H}_{nx}\left(\sigma_n^{(r)}, \mathcal{H}_{nx}\right) - \sigma_n^{(r)}\right) + \mathbf{b}_n.\mathbf{v}\right)\mathrm{d}\Omega \\ \mathbf{u}_n = \mathbf{u}_{in} \text{ on } \Gamma_4(t_n) \end{array} \right. \tag{40}$$

where $\mathbf{G}_{nx}$ is the gradient tensor of $\mathbf{H}_{nx}$. If for simplicity's sake we omit the subscripts n and x, then the components of the fourth-order tensor $\mathbf{G} = \mathbf{grad}_\sigma(\mathbf{H})$ are given by:

$$\forall (i,j,k,l) \in \{1,2,3\}^4 \;\; G_{ijkl} = \frac{\partial H_{ij}}{\partial \sigma_{kl}} \tag{41}$$

At last the iterations are stopped when the following inequality holds:

$$\left| \frac{\sigma_n^{(r+1)} - \sigma_n^{(r)}}{\sigma_n^{(r)}} \right| \leq e^{(tol)} \tag{42}$$

We shall now focus, in the following subsection, on the time discretization of the constitutive equations (2), (3), (5), (31) and (32).

3.3 Time discretization of the constitutive equations

The present subsection is devoted to the time discretization of the constitutive equations (2), (3), (5), (31) and (32). For that purpose two different time-discrete schemes have been implemented in the finite element program ELFIMTH developed in previous works for the numerical resolution of boundary value problems in thermomechanics.[10,11,12,13] They are described in the following paragraphs. But let us first make some general considerations.

To begin with note that the time-integration of the elastic component (3) of the strain rate tensor is immediate. And indeed, independently of the choice of any time-discrete scheme and taking into account the initial conditions (6.4b) and (6.4c), we have

$$\varepsilon^{(e)} = \mathbf{C} : (\sigma - \sigma_0) \tag{43}$$

On the other hand the thermal component (5) of the strain rate tensor will be approximated, with $\mathcal{O}(\Delta t_n^2)$ accuracy, by using the well-known Crank-Nicolson scheme, which gives

$$\varepsilon_n^{(th)} - \varepsilon_{n-1}^{(th)} = \frac{\alpha(T_{n-1}) + \alpha(T_n)}{2} (T_n - T_{n-1}) \mathbf{I}_2 \tag{44}$$

Eventually, let us put the following relations, which will be useful for the determination of the gradient tensor $\mathbf{G}$ defined in the previous subsection 3.2. For that purpose let $\mathbf{A}$ be the fourth-order tensor defined by

$$\mathbf{A} = \mathbf{I}_4 - \frac{1}{3}\mathbf{I}_2 \otimes \mathbf{I}_2 \tag{45}$$

where $\mathbf{I}_4$ denotes the fourth-order unit tensor. We then have $\mathbf{s} = \mathbf{A} : \sigma = \sigma : \mathbf{A}$. Thus,

$$\frac{\partial \mathbf{s}}{\partial \sigma} = \mathbf{A} \tag{46}$$

From $\mathbf{A} : \mathbf{A} = \mathbf{A}$ we get

$$\frac{\partial \left\|\mathbf{s}\right\|^2}{\partial \sigma} = 2\mathbf{s} : \mathbf{A} = 2\mathbf{s} \tag{47}$$

and then

$$\frac{\partial \left\|\mathbf{s}\right\|}{\partial \sigma} = \frac{\mathbf{s}}{\left\|\mathbf{s}\right\|} = \mathbf{d_s} \tag{48}$$

We have also

$$\left\{ \begin{array}{rcl} \dfrac{\partial \mathbf{d_s}}{\partial \sigma} & = & \dfrac{1}{\left\|\mathbf{s}\right\|}\mathbf{A} - \dfrac{1}{\left\|\mathbf{s}\right\|^2}\mathbf{s} \otimes \mathbf{d_s} \\ & = & \dfrac{1}{\left\|\mathbf{s}\right\|}\left(\mathbf{A} - \mathbf{d_s} \otimes \mathbf{d_s}\right) \end{array} \right. \tag{49}$$

On the other hand, the following relation

$$\left\{ \begin{array}{rcl} \dfrac{\partial \mathrm{tr}\left(\mathbf{s}^3\right)}{\partial \sigma} & = & \dfrac{\partial \left(s^{ij}s^{jk}s^{ki}\right)}{\partial \mathbf{s}} \dfrac{\partial \mathbf{s}}{\partial \sigma} \\ & = & 3\left(\mathbf{s}.\mathbf{s}\right) : \mathbf{A} \\ & = & 3\mathbf{s}.\mathbf{s} - \left\|\mathbf{s}\right\|^2 \mathbf{I}_2 \end{array} \right. \tag{50}$$

together with relation (48) leads to

$$\left\{\begin{array}{rcl}\dfrac{\partial \mathrm{tr}\left(\mathbf{d_s^3}\right)}{\partial\sigma} & = & \dfrac{\partial}{\partial\sigma}\dfrac{\mathrm{tr}\left(\mathbf{s}^3\right)}{\|\mathbf{s}\|^3} \\ & = & \dfrac{1}{\|\mathbf{s}\|^3}\left(3\mathbf{s}.\mathbf{s}-\|\mathbf{s}\|^2\mathbf{I}_2\right)-3\dfrac{\mathrm{tr}\left(\mathbf{s}^3\right)}{\|\mathbf{s}\|^4}\dfrac{\mathbf{s}}{\|\mathbf{s}\|} \\ & = & \dfrac{3}{\|\mathbf{s}\|}\left(\mathbf{d_s}.\mathbf{d_s}-\dfrac{1}{3}\mathbf{I}_2-\mathrm{tr}\left(\mathbf{d_s^3}\right)\mathbf{d_s}\right)\end{array}\right. \tag{51}$$

Let now $m=\max\{\sigma_1,\sigma_2,\sigma_3\}$. Then m is a zero of the following polynomial of degree 3

$$P(\sigma,m)=-m^3+I_1m^2-I_2m+I_3 \tag{52}$$

where I_1, I_2 and I_3 are defined by

$$\left\{\begin{array}{rcl}I_1 & = & \mathrm{tr}\sigma \\ I_2 & = & \dfrac{1}{2}\left(I_1^2-\mathrm{tr}\left(\sigma^2\right)\right) \\ I_3 & = & \det\sigma=\dfrac{1}{3}\mathrm{tr}\left(\sigma^3\right)-\dfrac{1}{2}I_1\mathrm{tr}\left(\sigma^2\right)+\dfrac{1}{6}I_1^3\end{array}\right. \tag{53}$$

The derivatives of those scalar invariants with respect to σ are as follows:

$$\left\{\begin{array}{rcl}\dfrac{\partial I_1}{\partial\sigma} & = & \mathbf{I}_2 \\ \dfrac{\partial I_2}{\partial\sigma} & = & I_1\mathbf{I}_2-\sigma \\ \dfrac{\partial I_3}{\partial\sigma} & = & \sigma.\sigma-I_1\sigma+I_2\mathbf{I}_2\end{array}\right. \tag{54}$$

Let us first assume that $\exists!\, i\in\{1,2,3\}$ such that $\sigma_i=m$. Then the total differentiation of $P(\sigma,m)=0$ gives

$$\frac{\partial P}{\partial\sigma}+\frac{\partial P}{\partial\, m}\frac{\partial m}{\partial\sigma}=0 \tag{55}$$

This relation together with relations (54) lead to

$$\frac{\partial m}{\partial\sigma}=\frac{\sigma.\sigma+\left(m-I_1\right)\sigma+\left(m^2-mI_1+I_2\right)\mathbf{I}_2}{3m^2-2mI_1+I_2} \tag{56}$$

Now, if $\exists!\,(i,j)\in\{1,2,3\}^2$, $i<j$, such that $\sigma_i=\sigma_j=m$ then m, which is a zero of $P(m,\sigma)$, is also a zero of the polynomial of degree 2 $P'(m,\sigma)=\partial P/\partial m$. In this particular case $\partial m/\partial\sigma$ is indeterminate and cannot be got from the previous relation (56). However a mean value of this derivative can be obtained by restricting σ to the set $S=\{\sigma;\exists!\,(i,j)\in\{1,2,3\}^2, i<j, \text{with } \sigma_i=\sigma_j=m\}$, for which the relation $P'(\sigma,m)=0$ holds. Taking into account relations (54), the total differentiation of this relation gives,

$$\frac{\partial m}{\partial\sigma}=\frac{\sigma+\left(2m-I_1\right)\mathbf{I}_2}{2\left(3m-I_1\right)} \tag{57}$$

Finally, if $\sigma_1=\sigma_2=\sigma_3=m$ then m, which is a zero of $P(m,\sigma)$ and $P'(m,\sigma)$, is also a zero of the ploynomial of degree 1 $P''(m,\sigma)=\partial^2P/\partial m^2$. In that case $\partial m/\partial\sigma$ is again indeterminate

and cannot be obtained from relations (56) or (57) as previously, but a mean value can be got by considering the set $S = \{\sigma; \sigma_1 = \sigma_2 = \sigma_3 = m\}$, for which we have $P''(\sigma, m) = 0$. The total differentiation of this equality together with the first of relations (54) leads to

$$\frac{\partial m}{\partial \sigma} = \frac{1}{3}\mathbf{I}_2 \tag{58}$$

The following paragraphs focus on the time discretization of the viscoplastic component (4) of the strain rate tensor.

3.3.1 Use of the θ-scheme for the time dicretization of $\dot{\varepsilon}^{(vp)}$

For the sake of conciseness we first consider the following ordinary differential equation $\dot{y}(t) = f(y,t)$. The use of the θ-scheme for its time-dicretization over the interval $[t_{n-1}, t_n]$ gives

$$y_n - y_{n-1} = \Delta t_n \left((1-\theta) f(y_{n-1}, t_{n-1}) + \theta f(y_n, t_n)\right) \tag{59}$$

where $\theta \in [0,1]$. If $\theta = 0$ we get the fully explicit Euler scheme, if $\theta = 1$ the fully implicit one, and if $\theta = 1/2$ the Crank-Nicolson scheme. It is well known that the θ-scheme has $\mathcal{O}(\Delta t_n^2)$ accuracy if $\theta = 1/2$ and $\mathcal{O}(\Delta t_n)$ if not. In other terms the previous approximation (59) of $y(t_n)$ has $\mathcal{O}(\Delta t_n^3)$ accuracy if $\theta = 1/2$ and $\mathcal{O}(\Delta t_n^2)$ if not. On the other hand, when f is linear then the θ-scheme is unconditionally stable if $\theta \geq 1/2$ and unconditionally superstable (i.e. stable without any oscillation) if $\theta = 1$. If $\theta < 1/2$ (resp. $\theta \neq 1$) then the time step Δt_n must take sufficiently small values in order to ensure the stability (resp. the superstability).

So the use of this classical scheme for the time discretization of the viscoplastic component $\dot{\varepsilon}^{(vp)}$ coming from relations (31) and (32) gives

$$\varepsilon_n^{(vp)} - \varepsilon_{n-1}^{(vp)} = \Delta t_n \left((1-\theta)\mathbf{F}(\sigma_{n-1}, T_{n-1}) + \theta \mathbf{F}(\sigma_n, T_n)\right) \tag{60}$$

By omitting the space variable x and taking into account relations (43) and (44), this leads to the following expression of the formal relation (37)

$$\left\{\begin{array}{rcl} \varepsilon_n & = & \mathbf{H}_n\left(\sigma_n, \mathcal{H}_n\right) \\ & = & \mathbf{C} : (\sigma_n - \sigma_{n-1}) + \Delta t_n \left((1-\theta)\mathbf{F}(\sigma_{n-1}, T_{n-1}) + \theta \mathbf{F}(\sigma_n, T_n)\right) \\ & + & \dfrac{\alpha(T_{n-1}) + \alpha(T_n)}{2}\left(T_n - T_{n-1}\right)\mathbf{I}_2 + \varepsilon_{n-1} \end{array}\right. \tag{61}$$

Let us now reconsider the expressions (31), (32), (49), (51), (56), (57) and (58) together with the first of relations (54). Then the fourth-order tensor $\mathbf{G}_n = \mathbf{grad}_\sigma(\mathbf{H_n})$ defined by (41) and relating to the iteration (r) takes the following form

$$\mathbf{G}_n\left(\sigma_n^{(r)}, \mathcal{H}_n\right) = \mathbf{C} + \theta \Delta t_n \phi_1\left(\sigma_n^{(r)}, T_n\right)\left[\mathbf{G}_1\left(\sigma_n^{(r)}, \mathcal{H}_n\right) + \mathbf{G}_2\left(\sigma_n^{(r)}, \mathcal{H}_n\right) + \mathbf{G}_3\left(\sigma_n^{(r)}, \mathcal{H}_n\right)\right] \tag{62}$$

where the scalar function ϕ_1 is given by the first of relations (32). As to the fourth-order tensorial functions $\mathbf{G}_1$, $\mathbf{G}_2$ and $\mathbf{G}_3$ of $\sigma_n^{(r)}$ and of the memory parameters $\mathcal{H}_n$, they are given by the following expressions, in which $\sigma_n^{(r)}$ has been replaced by σ for the sake of simplicity.

$$\left\{\begin{array}{rcl} \mathbf{G}_1\left(\sigma, \mathcal{H}_n\right) & = & \dfrac{C_4}{\|s\|}\left[C_1 - C_2 \mathrm{tr}(\mathbf{d}_\mathbf{s}^3)\right]\left[\phi_2(\sigma, T_n) - \delta(T_n)\right]\left[\mathbf{I}_4 - \dfrac{1}{3}\mathbf{I}_2 \otimes \mathbf{I}_2 - \mathbf{d}_\mathbf{s} \otimes \mathbf{d}_\mathbf{s}\right] \\ \mathbf{G}_2\left(\sigma, \mathcal{H}_n\right) & = & \dfrac{3C_2}{\|s\|}\left[\phi_2(\sigma, T_n) - \delta(T_n)\right]\left[C_3\mathbf{I}_2 - C_4\mathbf{d}_\mathbf{s}\right] \otimes \left[\mathbf{d}_\mathbf{s}.\mathbf{d}_\mathbf{s} - \dfrac{1}{3}\mathbf{I}_2 - \mathrm{tr}(\mathbf{d}_\mathbf{s}^3)\mathbf{d}_\mathbf{s}\right] \\ \mathbf{G}_3\left(\sigma, \mathcal{H}_n\right) & = & \dfrac{\phi_2(\sigma, T_n)}{\beta(T_n, c_p)\sigma_u}\left[C_1 - C_2 \mathrm{tr}(\mathbf{d}_\mathbf{s}^3)\right]\left[C_3\mathbf{I}_2 - C_4\mathbf{d}_\mathbf{s}\right] \otimes \left[\mathbf{I}_2 - (2+\alpha)\dfrac{\partial m}{\partial \sigma}\right] \end{array}\right. \tag{63}$$

The expressions of C_1, C_2, C_3, C_4, α and ϕ_2 are detailed in (32). Finally let us remind the reader that $m = \max\{\sigma_1, \sigma_2, \sigma_3\}$, where σ_1, σ_2 and σ_3 are the principal stresses, and that $\partial m/\partial\sigma$ is given by the relation (56) if $\exists!\, i \in \{1,2,3\}$ such that $\sigma_i = m$, by (57) if $\exists!\, (i,j) \in \{1,2,3\}^2$, $i < j$, such that $\sigma_i = \sigma_j = m$, and by (58) if $\sigma_1 = \sigma_2 = \sigma_3 = m$.

3.3.2 Direct integration of $\dot{\varepsilon}^{(vp)}$

This scheme is based on the following $\mathcal{O}(\Delta t_n^2)$-accurate approximation of $\sigma(t)$

$$\forall t \in [t_{n-1}, t_n],\ \sigma(t) = \sigma_{n-1} + \frac{\sigma_n - \sigma_{n-1}}{t_n - t_{n-1}}(t - t_{n-1}) + \mathcal{O}(\Delta t_n^2) \tag{64}$$

For the sake of simplicity, we shall consider that the value of the temperature used to compute the parameters β, γ and δ in equation (31) is constant on each interval $]t_{n-1}, t_n[$ and equal to $T_{n-\frac{1}{2}} = \frac{T_{n-1}+T_n}{2}$. Under this asumption, we will now omit the temperature dependence of the viscoplastic strain-rate and write, $\forall t \in]t_{n-1}, t_n[$:

$$\dot{\varepsilon}^{(vp)} = \mathbf{F}(\sigma, T) = \mathbf{F}\left(\sigma, T_{n-\frac{1}{2}}\right)$$

We will first describe the direct integration scheme by considering the following ordinary differential equation, where u and v play parts analogous to those of σ and ε, respectively

$$\dot{v}(t) = f(u(t)) \tag{65}$$

Then the previous approximation (64) gives :

$$\dot{v}(t) = f\left(u_{n-1} + \frac{u_n - u_{n-1}}{t_n - t_{n-1}}(t - t_{n-1})\right) + \mathcal{O}(\Delta t_n^2) \tag{66}$$

and the direct integration of equation (66) leads to :

$$v_n - v_{n-1} = \int_{t_{n-1}}^{t_n} f\left(u_{n-1} + \frac{u_n - u_{n-1}}{t_n - t_{n-1}}(t - t_{n-1})\right) \mathrm{d}t \tag{67}$$

which is a $\mathcal{O}(\Delta t_n^3)$-accurate relation between u and v.

In the case of the constitutive equation (2), this scheme leads to the following expression of the formal relation (37):

$$\left\{\begin{array}{ll} \varepsilon_n & = \mathbf{H}_n(\sigma_n, \mathcal{H}_n) \\ \varepsilon_n & = \mathbf{C} : (\sigma_n - \sigma_{n-1}) + \displaystyle\int_{t_{n-1}}^{t_n} \mathbf{F}\left(\sigma_{n-1} + \frac{\sigma_n - \sigma_{n-1}}{t_n - t_{n-1}}(t - t_{n-1}), T_{n-\frac{1}{2}}\right) \mathrm{d}t \\ & \qquad + \dfrac{\alpha\left(T_{n-1}\right) + \alpha(T_n)}{2}(T_n - T_{n-1})\mathbf{I}_2 + \varepsilon_{n-1} \end{array}\right. \tag{68}$$

and the fourth-order tensor $\mathbf{G}_n = \mathbf{grad}_\sigma(\mathbf{H}_n)$ defined by (41) and relating to the iteration (r) has the following form :

$$\mathbf{G}_n\left(\sigma_n^{(r)}, \mathcal{H}_n\right) = \mathbf{C} + \int_{t_{n-1}}^{t_n} \frac{t - t_{n-1}}{t_n - t_{n-1}} \mathbf{grad}_\sigma \mathbf{F}\left(\sigma_{n-1} + \frac{\sigma_n^{(r)} - \sigma_{n-1}}{t_n - t_{n-1}}(t - t_{n-1}), T_{n-\frac{1}{2}}\right) \mathrm{d}t \tag{69}$$

in which we have, by setting

$$\sigma^{(r)}(t) = \sigma_{n-1} + \frac{\sigma_n^{(r)} - \sigma_{n-1}}{t_n - t_{n-1}}(t - t_{n-1}) \tag{70}$$

$$\begin{cases} \mathbf{grad}_\sigma \mathbf{F}\left(\sigma^{(r)}(t), T_{n-\frac{1}{2}}\right) = \phi_1\left(\sigma^{(r)}(t), T_{n-\frac{1}{2}}\right)\left[\mathbf{G}_1\left(\sigma^{(r)}(t), T_{n-\frac{1}{2}}\right) + \mathbf{G}_2\left(\sigma^{(r)}(t), T_{n-\frac{1}{2}}\right)\right. \\ \qquad\qquad \left. + \mathbf{G}_3\left(\sigma^{(r)}(t), T_{n-\frac{1}{2}}\right)\right] \end{cases} \tag{71}$$

where $\mathbf{G}_1$, $\mathbf{G}_2$ and $\mathbf{G}_3$ are computed from (63) after replacing σ by $\sigma^{(r)}(t)$ and T_n by $T_{n-\frac{1}{2}}$. Both integrals defined by equations (68) and (69) are evaluated by using the Gauss-Legendre quadrature method.

4 Numerical simulations

In order to compare the different schemes presented in section (3.3), two problems have been simulated. The first one is an axisymmetric triaxial test. It is aimed to validate the schemes and to compare their accuracy and stability. The second one is a thermomechanical loading of a road, under the same conditions as a real-size test made by the LAVOC of the EPFL. It allows us to test the finite-element program on a real problem by comparing numerical results to experimental data. In the corresponding section, the temperatures are given in °C for clarity's sake.

4.1 Axisymmetric triaxial test

In this subsection, which only deals with compression tests, the sign conventions of the soil mechanics will be used for stresses and strains. We shall then consider that stresses are positive in compression and negative in traction. Consequently, positive strains represent contractions, whereas negative strains represent extensions.

The first series of computations are aimed to simulate an homogenous axisymmetric triaxial test on a cylindrical sample of bituminous concrete. It is divided into two phases: first, a constant strain rate is applied on the top of the sample in order to compress it. Then, when a strain level equal to 4.0 % is reached, a relaxation phase is simulated. These tests are conducted under a controlled constant temperature of 23 °C, and the mechanical parameters are chosen to simulate a material similar to the one used by Yan.[4] For the elastic part, Young modulus is $E = 600$ MPa and Poisson ratio is $\nu = 0.3$. For the viscoplastic part, the two constants defining the criterion are $\alpha_c = 2.25$ and $\alpha_t = 3.15$, the compactness of the concrete is $c_p = 93.6\,\%$ and the tangent Poisson ratio at viscoplastic flow is $\nu_\infty = 1.0$. On account of the axisymmetry and of the homogeneity of the problem, the sample is modelled by a single four-node quadrilateral element corresponding to its quarter, as shown on figure 3. This figure also presents the boundary conditions.

In this subsection, we are interested in two properties of the different schemes: their stability and their accuracy. And indeed, it is well known that for viscous constitutive equations, implicit schemes show a better stability than explicit ones.[16,11,21,22] We also focused on second-order accurate schemes for which we are expecting a good accuracy.

4.1.1 Stability

In order to compare the stability of the different schemes, computations are made with increasing values of the time step. Since unstability appears during the viscoplastic flow, we only simulate the first phase of loading (compression at a constant strain rate).

There is no analytical solution of such a problem. In order to get a reference solution, called REF in the following, the axial stress σ_{22} is computed thanks to the classical fourth-order Runge-Kutta scheme (for instance, see Crouzeix and Mignot[23]) applied to the one-dimensional equation binding σ_{22} and ε_{22}. The high number of time steps (20000) is chosen so that a solution obtained with twice increments will differ from the previous one in no more than the machine accuracy.

Four schemes are used in these simulations: for the sake of simplicity, they will be referred to by the following acronyms: explicit Euler scheme EE (θ-scheme with $\theta = 0$), implicit Euler scheme IE ($\theta = 1$), Crank-Nicolson scheme CN ($\theta = 0.5$) and direct integration scheme DI. The loading is made with a constant strain rate of $\dot{\varepsilon}_{22} = 1\,\%\text{min}^{-1}$ and a time step of $\Delta t = 6\,\text{s}$, $\Delta t = 12\,\text{s}$, $\Delta t = 24\,\text{s}$ and $\Delta t = 48\,\text{s}$. The results are presented in table 1.

Table 1: Stability of the schemes

Δt	6 s	12 s	24 s	48 s
CN	good	good	corner	good
EE	divergence	divergence	divergence	divergence
IE	good	good	good	good
DI	good	good	corner	oscillations

In that table, the term "*corner*" stands for solutions with a stress peak during transition from elastic behaviour to viscoplastic behaviour (see figure 4.b). The reason is that the different schemes use various combinations of σ_{n-1} and σ_n in order to compute the next stress σ_n. If the former stress σ_{n-1} plays too big a part, the numerical solution is more elastic-like than the real response. This overestimation disappears at the next increment, when the elastic behaviour vanishes compared to the viscoplastic one.

The bad results obtained with the explicit Euler scheme are not surprising. This scheme is the only one without implicit component, and previous studies (Royis and al[13]) show that for such a problem the size of the time step must not be greater than 2.4 s in order to avoid divergence. The performances of implicit Euler scheme, Crank-Nicolson scheme and direct-integration scheme are similar to those observed by Royis[11, 21, 22] for linear and non-linear viscoelastic constitutive equations. As an example, strain-stress curves are presented for explicit Euler scheme (figure 4.a), implicit Euler scheme, Crank-Nicolson scheme and direct integration scheme (figure 4.b) for $\Delta t = 24\,\text{s}$.

4.1.2 Accuracy

The second step to compare the schemes is to evaluate their precision on a simple problem. Once again, the axisymmetric triaxial test described at the beginning of subsection 4.1 has been chosen. Let us recall that this test is divided into two phases: first, a vertical contracting displacement is applied onto the sample at a constant strain rate. When a strain $\varepsilon_{22} = 4\,\%$ is reached, the head of the sample is prevented from moving in order to let the bituminous concrete relax. This condition is maintained until the end of the test which lasts 2100 s. As for the previous test, an analytical solution cannot be found out. The reference solution is then given by the application of the classical fourth-order Runge-Kutta method to the one-dimensional constitutive equation binding σ_{22} and ε_{22}, with as many time steps as required to get scheme-imprecision lower than computer's round-off error, that is with 14000 time steps. Comparisons between the four schemes are made with three different strain-rates: $\dot{\varepsilon}_{22} = 0.25\,\%\text{min}^{-1}$, $\dot{\varepsilon}_{22} = 1.0\,\%\text{min}^{-1}$ and $\dot{\varepsilon}_{22} = 4.0\,\%\text{min}^{-1}$. The time step size is equal to $\Delta t = 1.2\,\text{s}$ to avoid unstability problems. Each simulation is then computed with 1750 time steps. For each scheme, the relative error is computed with:

$$e_n = \left| \frac{\sigma_{22n}^{(num)} - \sigma_{22n}^{(ref)}}{\sigma_{22n}^{(ref)}} \right| \tag{72}$$

where for each time t_n, e_n is the error, $\sigma_{22n}^{(num)}$ is the axial stress obtained by the finite element program and $\sigma_{22n}^{(ref)}$ is the one given by the reference solution. For each scheme and for each value of $\dot{\varepsilon}_{22}$, the table 2 gives the maximum of the relative error.

Table 2: Precision of the schemes

$\dot{\varepsilon}_{22}$	$0.25\,\%\text{min}^{-1}$	$1.0\,\%\text{min}^{-1}$	$4.0\,\%\text{min}^{-1}$
CN	$9.92\,10^{-5}$	$4.22\,10^{-4}$	$4.50\,10^{-3}$
EE	$4.70\,10^{-3}$	$1.21\,10^{-2}$	$1.17\,10^{-1}$
IE	$4.60\,10^{-3}$	$1.12\,10^{-2}$	$2.75\,10^{-2}$
DI	$9.92\,10^{-5}$	$2.28\,10^{-4}$	$2.20\,10^{-3}$

We first note that the error increases for higher strain-rate, whatever the scheme is. The theory predicted that second-order accurate schemes would give better results than first-order accurate ones. It can be seen in table 2: implicit and explicit Euler schemes give errors 50 times bigger than the other ones. Moreover, direct integration scheme seems to be slightly better than Crank-Nicolson one. As an instance, the relative error e_n versus time is shown for implicit Euler scheme (figure 5.a) and Crank-Nicolson scheme (figure 5.b) with $\dot{\varepsilon}_{22} = 0.25\,\%\text{min}^{-1}$.

As shown on figure 5, the relative error reaches its maximum during the beginning of the relaxation phase. It is equal to zero during the viscoplastic flow in the compression phase, and remains sligthly oscillating at the end of relaxation phase.

4.1.3 Computation speed

The ultimate goal, when developing various integration schemes, is to increase the speed of the computations without losing any precision. The speed of a computation depends on two

parameters: the number of time steps used to run the simulation, and the number of iterations required to obtain the convergence of the Newton method in each time-step. Let us point out here that the convergence is assumed to be obtained as soon as the relative difference (42) between two successive stress fields becomes lower than 10^{-6}. Moreover, let us remind the reader that for explicit Euler scheme EE the convergence is obtained after the first iteration. To be rigorous, we have to take into account the duration of an iteration for the various schemes. The previous simulations performed on the same computer showed that this duration is approximatively the same (around a quarter of second), whatever the scheme employed is. This means that the finite element processing and files operations make the difference in number of basic operations negligible for the different schemes considered.

The two former subsections showed the good properties of the three non-explicit schemes EI, CN and DI. For a given size Δt of the time-step, the total number of iterations required by each of these three schemes allow us to compare their computation speed. These results are presented in table 3, for the same problem as in subsection 4.1.1 (homogenous axisymmetric triaxial test in compression) with the same boundary conditions.

Table 3: Total number of iterations for different values of the time step

Δt	1.2 s	6 s	12 s	24 s	48 s
CN	419	88	54	45	38
IE	438	114	72	57	36
DI	421	89	54	47	*

* Not computed because oscillating

This table shows the better behaviour of second-order schemes CN and DI, which converge faster than the first-order scheme EI. But when Δt becomes too big (48 s), the oscillations in CN make the convergence harder to obtain, whereas IE (which is superstable) becomes as fast as the second-order scheme CN.

As shown in subsection 4.1.2, the second advantage of second-order schemes is their higher precision. For instance, for $\Delta t = 6\,\mathrm{s}$, the relative error (72) can be computed, thanks to the "reference solution" given by the Runge-Kutta method with 20000 time steps. It is worth $3.705\,10^{-3}$ for CN and $2.989\,10^{-3}$ for DI. By comparison, 500 time steps of 1 iteration each are required to obtain similar precison with the explicit Euler scheme EE, as shown in table 4.

Table 4: Relatives errors of EE for different values of the time step

Δt	1.2 s	0.6 s	0.48 s	0.3 s
Nb of increments	200	400	500	800
Relative error	$9.633\ 10^{-3}$	$4.779\ 10^{-3}$	$3.829\ 10^{-3}$	$2.389\ 10^{-3}$

In other terms, for the problem considered schemes CN and DI allow us to obtain the same precison as EE 5.6 times faster.

4.2 Thermomechanical loading of a road structure

Bituminous concrete is widely used in road construction. So it seems natural to use our finite-element program to simulate the behaviour of a road structure. This simulation is based on a real-size experiment performed at the LAVOC in 1991[24] and 1992.[25] The experimental data are presented in the report of the LAVOC.[6] In this subsection, the sign conventions of the continuum mechanics will be used: stresses are positive for tractions and negative for compressions, positive strains represent extensions and negative strains represent contractions.

4.2.1 Presentation

The structure consists of three rectangular layers (4m × 5m), as can be seen on figure 6.

The first one is bituminous concrete, called BC on that figure, and is 8 cm thick. We model it with the previous constitutive equations (2), (3), (5), (31) and (32). Its mechanical parameters are the same as for the previous tests (described in subsection 4.1). The second layer is made of GRECO (Groupement de REcherches COordonnées) sand (called sand 1 on the figure) and is 80 cm thick. The last one is of La Saubraz sand (sand 2) and is 120 cm thick. Both sands are governed by the same incremental law involving interpolations together with a Drucker-Prager criterion. Let us notice that the study of such a law is not within the scope of the paper. For details, the reader may refer to Royis. [26,11] The mechanical parameters for both materials are: initial tangent modulus $E_0 = 253\,\text{MPa}$, initial tangent Poisson ratio $\nu_0 = 0.23$, tangent Poisson ratio at the plastic flow for compression axisymmetric triaxial test $\nu_a = 0.7$, cohesion $C = 0$ and friction angle $\psi = 45^o$. In order to simulate the thermal behaviour of materials, we also need the following values: mass density ρ (kg.cm^{-3}), thermal conductivity λ_T (W.cm^{-1}.°C^{-1}) –which can be temperature-dependent–, heat capacity at constant volume c_T (J.kg^{-1}.°C^{-1}) and coefficient of thermal expansion α (°C^{-1}). The values used in the program are given in table 5 (the temperatures are given in °C).

Table 5: Numerical values of thermal parameters

Material	ρ kg.cm^{-3}	T °C	λ_T W.cm^{-1}.°C^{-1}	c_T J.kg^{-1}.°C^{-1}	α °C^{-1}
Bituminous concrete	$2.2785\,10^{-3}$	7	$6.923\,10^{-3}$	759	$4.85\,10^{-5}$
		15	$9.231\,10^{-3}$		
		28	$9.532\,10^{-3}$		
Greco's sand	$1.4697\,10^{-3}$	/	$1.03\,10^{-2}$	917	0
La Saubraz' sand	$1.5618\,10^{-3}$	/	$1.03\,10^{-2}$	917	0

The experiment consists of three phases: a thermal one, a mechanic one with quasistatic loadings and several temperature states, and a dynamic one. The last one will not be simulated here because the program used is not able to take dynamic effects into account. The thermal boundary conditions, described further, are such that the temperature state at a given time

depends only on the depth. Two rigid discs (called I and II) are used to load the structure. Their diameter is 30 cm. We focus on the zone around one disc (disc I). When this disc is used, the other one is unloaded. Moreover, since the distance between the two axes is 180 cm, the effects of the previous loadings through disc II on the memory parameters of the materials near disc I may be neglected. The axis of disc I is 160 cm far from the closest border, so the border effects can be neglected too. Then we shall assume that the problem is axisymmetric. The radial half-plane of a cylinder with the same axis as the disc I is discretized with the help of a 200 four-node quadrilateral elements mesh with 429 degrees of freedom. This cylinder is 208 cm high and its radius is 220 cm so as to ensure that the stresses and the strains are equal to 0 at the points 160 cm far from the axis (closest border of the road structure).

The mesh is represented on figure 6. The thermal boundary conditions are of two types: Dirichlet conditions on side BC (a cooling system sets the temperature at 10 °C), Neumann conditions on sides AB (symmetry of the problem) and CD (insulated border). As to side DA (convection between air and road surface), the simplest hypothesis has been taken: since it is very difficult to set a good convective surface heat transfer coefficient, we decided to consider that the bituminous concrete temperature on the surface was the same as the air temperature. Computations with both Dirichlet and Fourier conditions have been made and the specified temperature condition gave the best results in comparison with experimental data. For the mechanical problem, we set: on sides AB, BC and CD, normal displacement $\mathbf{u}_i \cdot \mathbf{n} = 0$ and tangential stress $\mathbf{g} \cdot \mathbf{t} = 0$ (where $\mathbf{t}$ is directly orthogonal to the normal $\mathbf{n}$). On side DA, the stress vector is null except under the loading disc where $\mathbf{g} = -\frac{F}{S}\mathbf{e}_z$, with $S = 706.86\,\text{cm}^2$ the area of the disc and F the global force applied on that disc. The mesh and the boundary conditions for the mechanical problem are represented on figure 6.

4.2.2 Thermal loading

The first phase of the test conducted in the LAVOC consisted in having air temperature varied between 21 °C, 5 °C and 40 °C and mesuring temperature in the different layers. The simulation is divided into 1312 time steps lasting about 2 hours each. The figure 7 compares experimental and numerical results for 4 different depths.

As can be seen on this figure, the simulation gives good results, despite the hypothesis about boundary conditions between air and road surface. The only noticeable difference is due to a failure in the temperature regulator at the end of the first phase in the LAVOC, which has not been modelled in our computation.

4.2.3 Mechanical loading

A rigid disc is used in order to apply a uniform stress on a part of the surface of the structure. LAVOC experiment consisted in four phases of loading, each of them applied under a constant temperature. Only one of these phases is presented here. The temperature of the air is maintained at 5 °C. This condition is set during 19 days, in order to get a time-independent temperature field in the road structure. So, as explained above, the temperature depends only on the depth. The mechanical loading (global force F) is then applied as shown on figure 8.

This phase is modelled by using the same 429-dof-mesh as above. Due to previous considerations, the problem is supposed to be axisymmetric. The boundary conditions are as above,

with specified temperature on side DA equal to 5 °C (air temperature) and force F given by figure 8. The Crank-Nicolson scheme has been used for the discretization of the constitutive equations of the bituminous concrete. Some results are given on figures 9 to 13. These figures show the strains obtained from the program (continued lines, referred to by numbers in brackets) compared with experimental data provided by the LAVOC (dotted lines, referred to by numbers in square brackets).

Figure 9 shows the radial strains under the axis of loading at the middle of the layer of bituminous concrete ($z = -4\,\text{cm}$) and at the interface between the bituminous concrete and the sand ($z = -8\,\text{cm}$). There are noticeable differences between numerical and experimental results, especially as regards $z = -4\,\text{cm}$. It may be due to the spatial discretization used in the program: strains are computed at the centre of each element, so the points used for experimental and numerical results are not exactly the sames. For instance, strains at the middle of the bituminous concrete are mesured at $r = 0$ and $z = -4$ by the LAVOC, and computed at $r = 1$ and $z = -4$ by the program (coordinates are given in centimeters).

Figures 10 and 11 show radial and orthoradial strains on the surface of the bituminous concrete for different values of the radius. In each case, the first point ($r = 4.5\,\text{cm}$) has been removed: the experimental data at that point seemed totally nonsensical. It may be due to the position of the corresponding captors. And indeed, they were under the disc, so they might have been damaged during the loading. As concerns the other captors, the program give fairly good results, the different curves show the same order of strains and the same shape. The differences in the numerical values can be explain as for figure 9: the experimental data represent strains on the surface of the road, whereas the numerical data are computed at the center of the first row of elements, that is at a depth of $z = -1\,\text{cm}$.

Eventually, figures 12 and 13 show radial and orthoradial strains at the interface between the bituminous concrete and the sand. Here, we can see that the program overestimates radial and orthoradial strains for small radii ($r = 0$ and $r = 4.5\,\text{cm}$), but gives good results for larger radii. One shall notice that, in this case, the strains are taken at the same points for both numerical and experimental results, that is exactly at the interface between bituminous concrete and sand, but in the case of the simulation, with a hypothesis of perfect sticking between both materials, which might explain the differences observed for small radii.

5 Conclusion

In order to model the thermoviscoplastic behaviour of bituminous concrete, a tensorial constitutive equation has been stated on the basis of one-dimensional relations coming from experimental results obtained at the LGM of the ENTPE, and then implemented in the finite element program ELFIMTH developed in previous works for the numerical resolution of boundary value problems in thermomechanics. That implementation was carried out by using two different time-discrete schemes for the numerical integration of the constitutive equations considered over finite time steps. A set of numerical simulations of homogeneous triaxial tests has shown the good properties of these schemes when compared with the classical fully explicit Euler one. The resulting finite element program was also used to simulate a real size experiment performed at the LAVOC of the EPFL. The comparison between numerical results and experimental data shows a fair agreement for that more complex and realistic problem, even if some discrepancies

can be observed. The future steps of the work presented in this paper will include[27] the bringing into play, for the constitutive equations considered, of an original time-discrete scheme recently developed for linear and non-linear viscoelastic models;[21,22] a more detailed study of the various time-discrete schemes implemented in the finite element program ELFIMTH, the numerical simulations of the others stages of the thermomechanical loadings performed on the real-size road structure of the LAVOC, and the study of the influence of those time-discrete schemes on the corresponding numerical results.

Acknowledgements

The work presented in this paper was partly supported by the "Geomaterials EUROGRECO".

References

1. D. Aubry, E. Bard, and A. Modaressi. A Mixture approach to the mechanical behaviour of bituminous concrete. In C. Desai and al., editors, *Constitutive laws for Engineering Materials*, 1987.

2. H. Di Benedetto. *Modélisation du comportement des géomatériaux - Application aux enrobés et aux bitumes*. Thèse de Doctorat ès Sciences Physiques, Université scientifique et médicale de Grenoble, Septembre 1987.

3. P.G. Bonnier, P.A. Vermeer, and J. Lindenberg. Creep behaviour of bituminous concrete. In S. Pietruszczak and G.N. Pande, editors, *Proceedings of the Fourth International Conference on Numerical Models in Geomechanics*. A.A. Balkema, 1992.

4. X.L. Yan. *Comportement mécanique des enrobés au bitume et au bitume polymère (Styrelf 13)*. Thèse de Doctorat (spécialité Génie Civil), Institut National des Sciences Appliquées de Lyon, Avril 1992.

5. H. Di Benedetto and X.L. Yan. Comportement mécanique des enrobés bitumineux et modélisation de la contrainte maximale. *Materials and Structures*, (27):539–547, 1994.

6. A.-G. Dumont, A. Salhi, E. Recordon, and I. Gueye. Validation expérimentale des lois de comportement de matériaux hydrocarbonés et de sols. Technical report, Laboratoire des Voies de Circulation, Laboratoire de Mécanique des Sols de l'Ecole Polytechnique Fédérale de Lausanne, 1994.

7. P. Perzina. The constitutive equations for rate sensitive plastic materials. *Quarterly of Applied Mathematics*, 20(4):321–332, 1963.

8. T. Adachi and F. Oka. Constitutive equations for normally consolidated clay based on elastoviscoplasticity. *Soils and Foundations*, 22(4):57–70, 1982.

9. F. Oka, A. Yashima, and S. Leroueil. An elasto-thermo-viscoplastic model for natural clay and its application. In S. Pietruszczak and G.N. Pande, editors, *Proceedings of the Sixth International Conference on Numerical Models in Geomechanics*, pages 105–110. A.A. Balkema, 1997.

10. P. Royis, Z.M. Chen, and N. Farges. A finite element formulation for non-linear analysis of thermo-viscoplastic problems. In A.B. Sabir and A. Niku-Lari, editors, *Proceedings of the International Conference FEMCAD CRASH 93*, pages 87–92, 1993.

11. P. Royis. *Modélisation par éléments finis des géomatériaux*. Thèse d'Habilitation à Diriger des Recherches (spécialité Mécanique et Energétique), Institut National Polytechnique de Grenoble, Mars 1995.

12. Z.M. Chen. *Modélisation par éléments finis du comportement mécanique des enrobés bitumineux*. Thèse de Doctorat (spécialité Génie Civil), Institut National des Sciences Appliquées de Lyon, Mai 1985.

13. P. Royis, J.F. Seignol, and Z.M. Chen. Numerical simulation by FEM of the thermoviscoplastic behaviour of bituminous concrete. In *Proceedings of the Fourth International Conference on Computational Plasticity, Fundamentals and Applications*, 1995.

14. S.W. Sloan. Substepping schemes for the numerical integration of elastoplastic stress-strain relations. *International Journal for Numerical Methods in Engineering*, 24:893–911, 1987.

15. S.W. Sloan and J.R. Booker. Integration of Tresca and Mohr-Coulomb constitutive relations in plane strain elastoplasticity. *International Journal for Numerical Methods in Engineering*, 33:163–196, 1992.

16. T.J.R. Hughes and R.L. Taylor. Unconditionally stable algorithms for quasi-static elasto-visco-plastic finite element analysis. *Computers and Structures*, 8:169–173, 1978.

17. M.L. Wenner. A generalized forward gradient procedure for rate sensitive constitutive equations. *International Journal for Numerical Methods in Engineering*, 36:985–995, 1993.

18. H.H. Rosenbrock. Some general implicit processes for the numerical solution of differential equations. *Comp. J.*, 5:329–330, 1963.

19. P. Royis. *Formulation mathématique de lois de comportement - Modélisation numérique de problèmes aux limites en mécanique des solides déformables*. Thèse de Doctorat d'Ingénieur (spécialité Mécanique), Institut National Polytechnique de Grenoble, Juillet 1986.

20. P. Royis. An original time-discrete scheme for viscoelastic and viscoplastic problems. In Cedex, editor, *Proceedings of the Second European Specialty Conference on Numerical Methods in Geotechnical Engineering*, pages 145–154, 1990.

21. P. Royis. Integration by FEM of viscous models: a comparison between three time-discrete schemes. In S. Pietruszczak and G.N. Pande, editors, *Proceedings of the Fifth International Conference on Numerical Models in Geomechanics*, pages 423–428. A.A. Balkema, 1995.

22. P. Royis. A superstable time-discrete scheme for the numerical integration of viscous constitutive equations. *Mechanics of Cohesive-Frictional Materials*, 1997.

23. M. Crouzeix and A.L. Mignot. *Analyse numérique des équations différentielles*. Masson, 1989.

24. P. Royis and al. Modélisation numérique des enrobés bitumineux. In F. Darve, editor, *Rapport scientifique 1991 de l'Euro-Greco Géomatériaux*, pages 19–38, 1991.

25. P. Royis and al. Modélisation numérique des enrobés bitumineux. In F. Darve, editor, *Rapport scientifique 1992 de l'Euro-Greco Géomatériaux*, pages 13–34, 1992.

26. P. Royis. Interpolations and one-to-one properties of incremental constitutive laws - A family of incrementally nonlinear constitutive laws. *European Journal of Mechanics A/solids*, 8(5):385–411, 1989.

27. J.F. Seignol. *Simulation par éléments finis du comportement thermoviscoplastique des bétons bitumineux*. Thèse de Doctorat (spécialité Mécanique des Solides), Institut National Polytechnique de Grenoble, à paraître en 1999.

Notations

ROMAN TYPE

Notation	Meaning
$\mathbf{A}$	fourth-order tensor binding σ and $\mathbf{s}$
$\mathbf{b}$	field of body forces per unit volume
C	cohesion of the sands
c_p	compactness of the bituminous concrete
$\mathbf{C}$	tensor of elastic compliances
C_1, C_2, C_3, C_4	four scalar functions of ν_∞
c_T	heat capacity at constant volume
$\mathbf{d}_{\dot{\varepsilon}^{(vp)}}$	direction of $\dot{\varepsilon}^{(vp)}$
$\mathbf{d}_{\mathbf{s}}$	direction of $\mathbf{s}$
$e^{(tol)}$	threshold of convergence
E	Young modulus of the elastic part of the bituminous concrete behaviour
E_0	initial tangent modulus of the sands
F	global force applied on the disc
$\mathbf{g}$	field of stress vectors prescribed on $\Gamma_5(t_n)$
$\mathbf{G}_{nx}$	gradient tensor of $\mathbf{H}_{nx}$
$\mathbf{G}_1$, $\mathbf{G}_2$, $\mathbf{G}_3$	fourth-order tensors, the sum of which contributes to $\mathbf{G}_{nx}$
h_T	convective suface heat transfer coefficient
$\mathbf{H}_{nx}$	constitutive function binding $\sigma_n(x)$, $\mathcal{H}_{nx}$ and $\varepsilon_n(x)$
$\mathcal{H}_{nx}$	memory parameters of the bituminous concrete
I_1, I_2, I_3	scalar invariants of σ
$\mathbf{I}_2$	second-order unit tensor
$\mathbf{I}_4$	fourth-order unit tensor
$\mathbf{n}$	outer unit normal to Γ
$(\mathbf{P}_{nv})$	weak formulation of the time-discretized mechanical problem relating to t_n
$(\mathbf{P}_{nh})$	finite element approximation of $(\mathbf{P}_{nv})$
$\left(\mathbf{P}_{nh}^{(r)}\right)$	linearization of $(\mathbf{P}_{nh})$ relating to iteration (r)
$\mathbf{q}$	vectorial field of heat flux
Q	field of internal heat generation per unit volume
$(\mathbf{Q}_n)$	time-discretized thermal problem relating to t_n
$(\mathbf{Q}_{nv})$	weak formulation of $(\mathbf{Q}_n)$
$(\mathbf{Q}_{nh})$	finite element approximation of $(\mathbf{Q}_{nv})$
$\left(\mathbf{Q}_{nh}^{(r)}\right)$	linearization of $(\mathbf{Q}_{nh})$ relating to iteration (r)
$\mathbf{s}$	deviatoric part of the stress tensor σ
S	area of the discs
t, t_n	time, time values
$\mathbf{t}$	unit vector directly orthogonal to the normal $\mathbf{n}$
T	temperature
T_i	temperature prescribed on $\Gamma_1(t_n)$
$T_n^{(r)}$	solution of $\left(\mathbf{Q}_{nh}^{(r)}\right)$
T_a	temperature of the ambient medium
$\mathbf{u}$	field of displacements
$\mathbf{u}_i$	field of displacements prescribed on $\Gamma_4(t_n)$
$\mathbf{u}_n^{(r)}$	solution of $\left(\mathbf{P}_{nh}^{(r)}\right)$

ROMAN TYPE (continued)

Notation	Meaning
V	Sobolev space $(\mathrm{H}^1(\Omega))^3$
V_h	finite element space, subset of V_n
V_n	$\{\mathbf{v} \in V, \mathbf{v}\|\Gamma_4(t_n) = 0\}$
W	Sobolev space $\mathrm{H}^1(\Omega)$
W_h	finite element space, subset of W_n
W_n	$\{w \in W\|w\|\Gamma_1(t_n) = 0\}$
Y	Heaviside function

GREEK TYPE

Notation	Meaning
$\alpha(T)$	coefficient of thermal expansion
α_c, α_t	positive constants defining the viscoplastic criterion
β, γ	scalar functions of T and c_p
δ	scalar function of T
Δt_n	time increment
ε	linearized tensorial field of small strains
$\dot{\varepsilon}$	strain rate tensor
$\dot{\varepsilon}_u$	unit of strain rate
$\dot{\varepsilon}^{(e)}$	elastic component of $\dot{\varepsilon}$
$\dot{\varepsilon}^{(th)}$	thermal component of $\dot{\varepsilon}$
$\dot{\varepsilon}^{(vp)}$	viscoplastic component of $\dot{\varepsilon}$
Γ	boundary of Ω
$\Gamma_1(t_n)$	part of Γ where the temperature is prescribed at time t_n
$\Gamma_2(t_n)$	part of Γ where the heat flux per unit area is prescribed at time t_n
$\Gamma_3(t_n)$	part of Γ where the heat flux is governed by convection at time t_n
$\Gamma_4(t_n)$	part of Γ where the displacement is prescribed at time t_n
$\Gamma_5(t_n)$	part of Γ where the stress vector is prescribed at time t_n
λ_T	thermal conductivity
ν	Poisson ration of the elastic part of the bituminous concrete behaviour
ν_0	initial Poisson ratio for the sands
ν_a	tangent Poisson ratio at plastic flow in compression for the sands
ν_∞	Poisson ratio at viscoplastic flow in compression for the bituminous concrete
φ	heat flux per unit area prescribed on $\Gamma_2(t_n)$
ψ	friction angle for the sands
ϕ	Lode angle
Ω	materially simple continuum, open region of $\mathbb{R}^3$
ρ	mass density
σ	tensorial field of the Cauchy stresses
σ_u	unit of stress
σ_1, σ_2, σ_3	principal stresses
$\sigma_1^{(c)}$	breaking axial stress for axisymmetric triaxial tests in compression
$\sigma_1^{(cr)}$	residual axial stress after relaxation for axisymmetric triaxial tests in compression

List of Figures

List of Tables

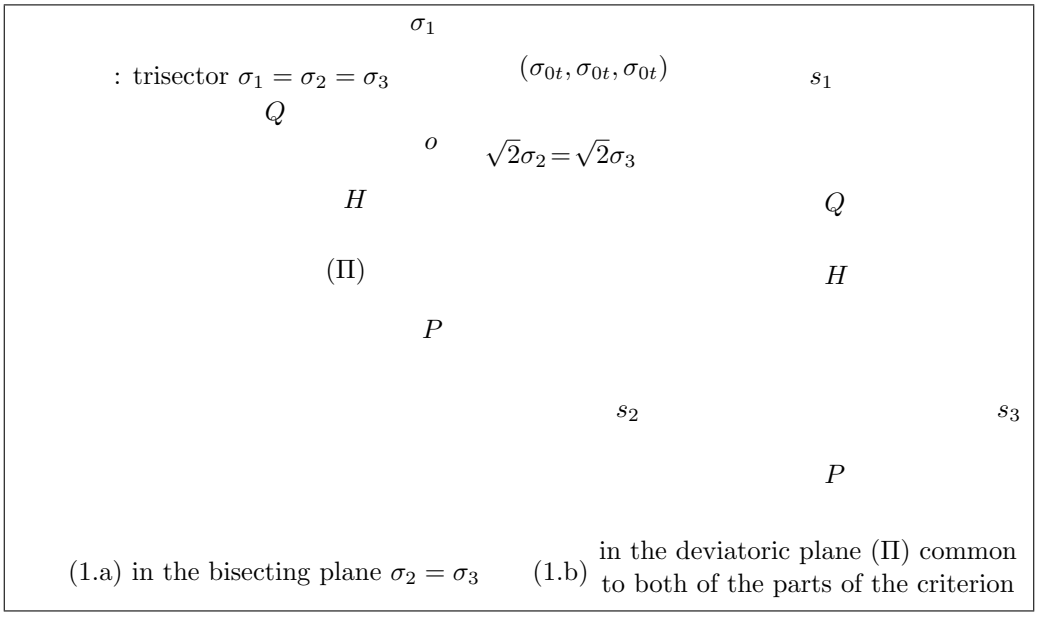

Figure 1: Geometrical shape of the viscoplastic criterion proposed by Di Benedetto

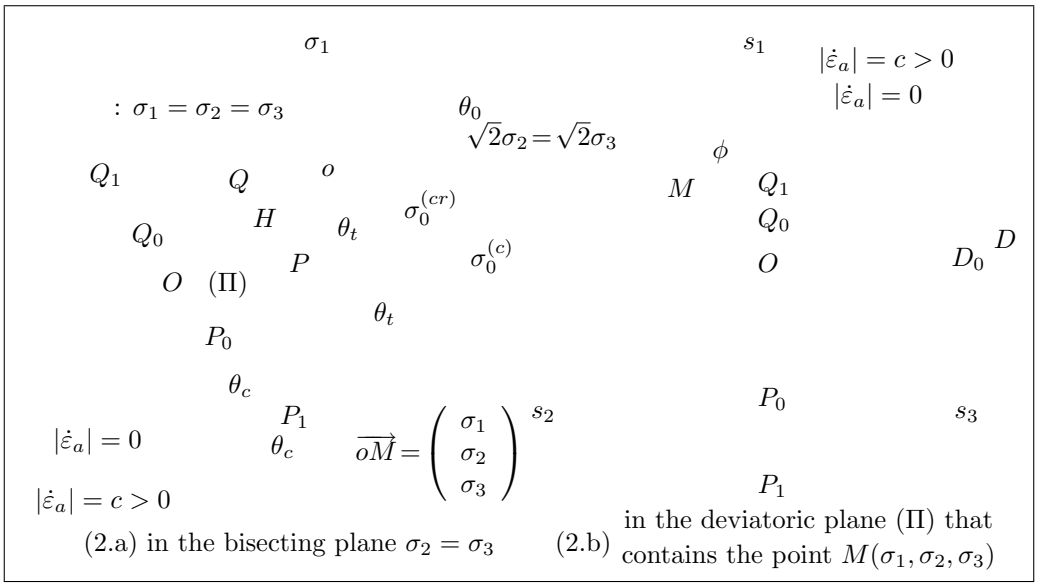

Figure 2: A surface of breaking stresses obtained by similarity from the viscoplastic criterion

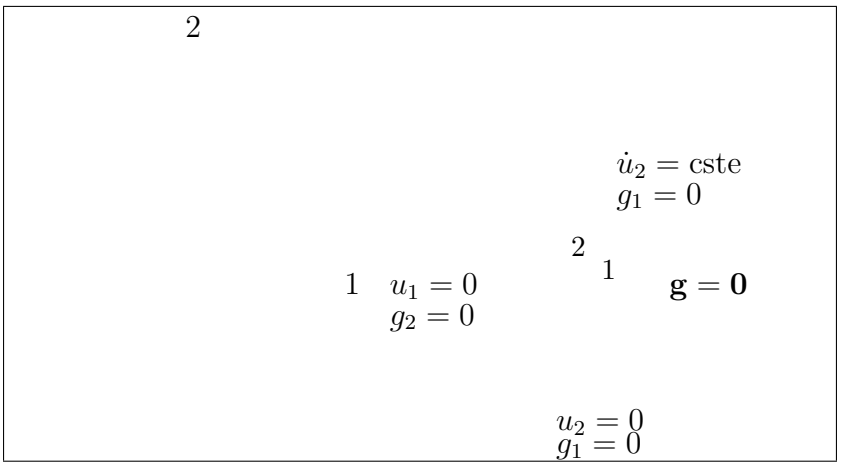

Figure 3: Boundary conditions for triaxial test

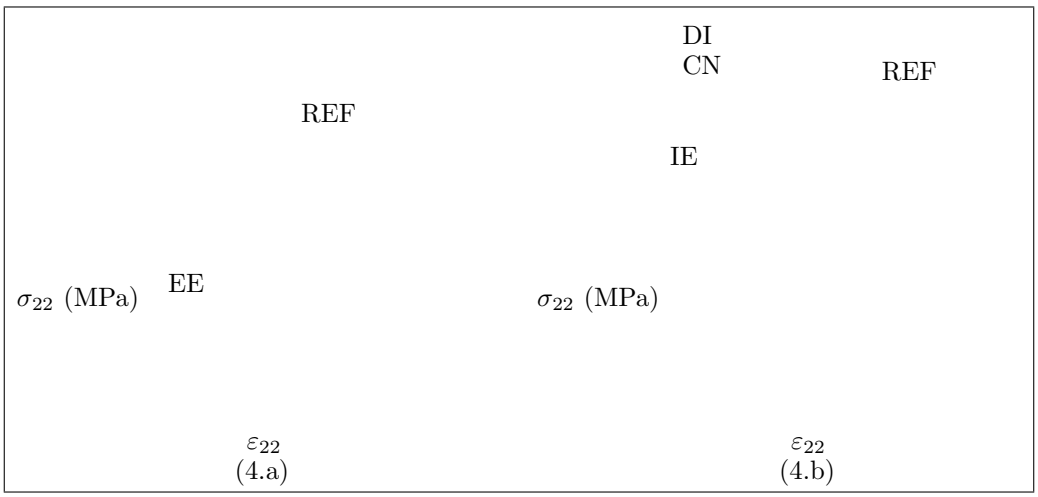

Figure 4: Axial stress σ_{22} versus axial strain ε_{22} for $\Delta t = 24$s

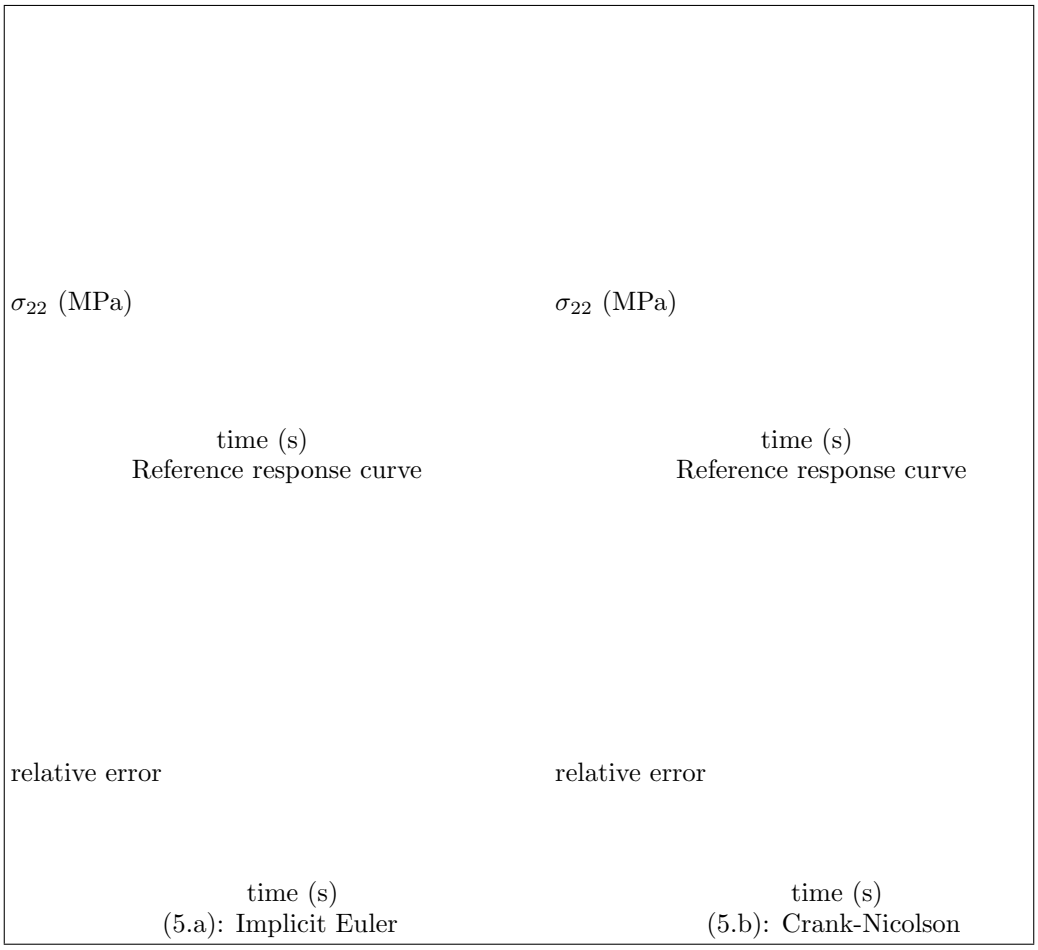

Figure 5: Relative error ($\dot{\varepsilon}_{22} = 0.25\,\%\text{min}^{-1}$)

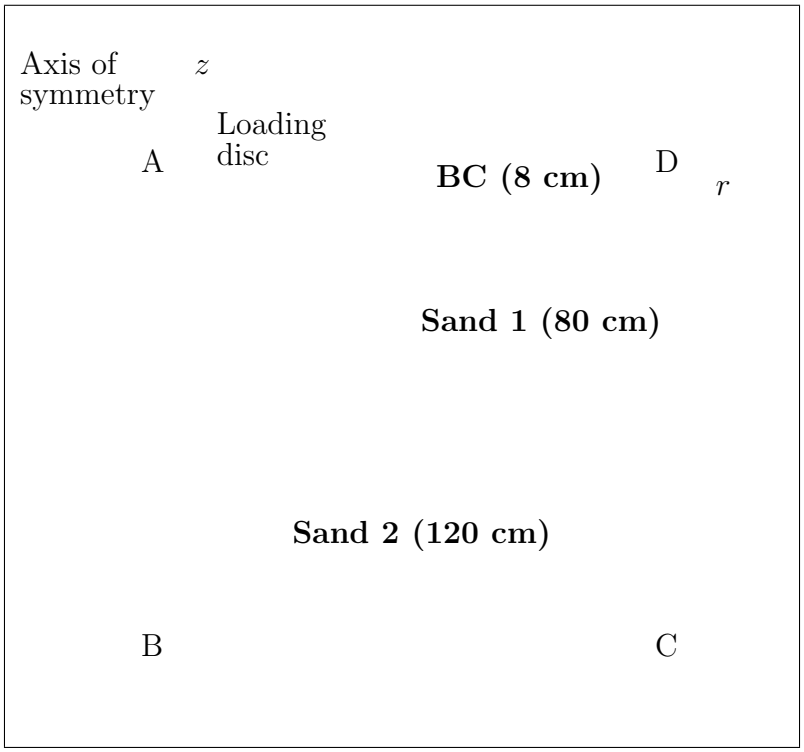

Figure 6: Boundary conditions and mesh for the road structure

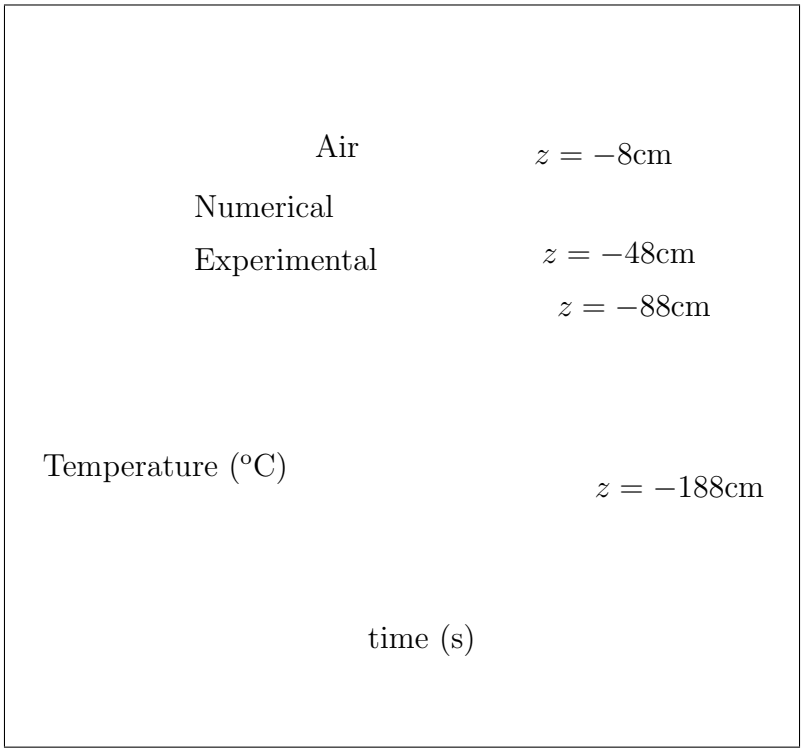

Figure 7: Comparison between numerical and experimental results for the first phase

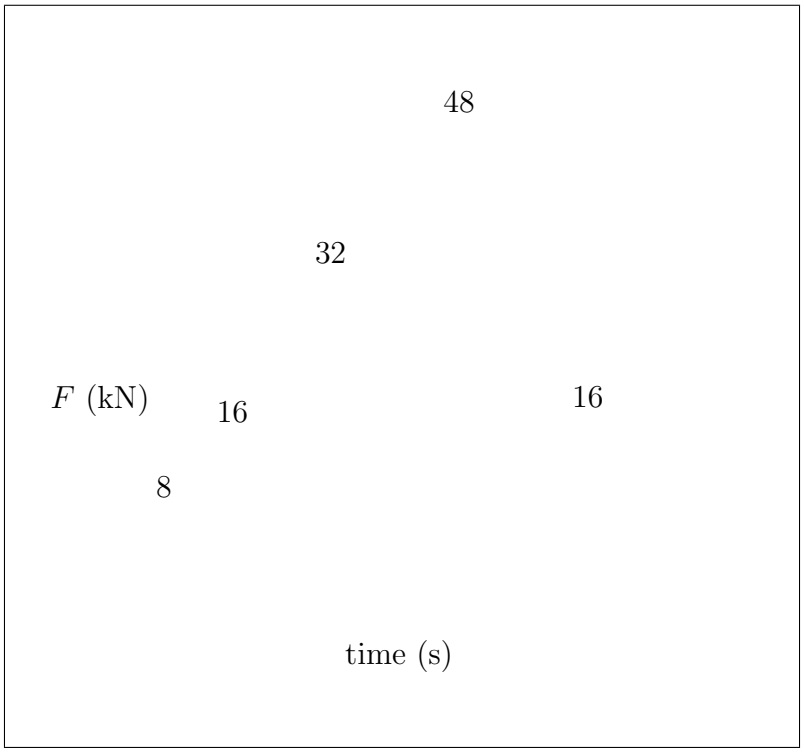

Figure 8: Global force applied on the disc

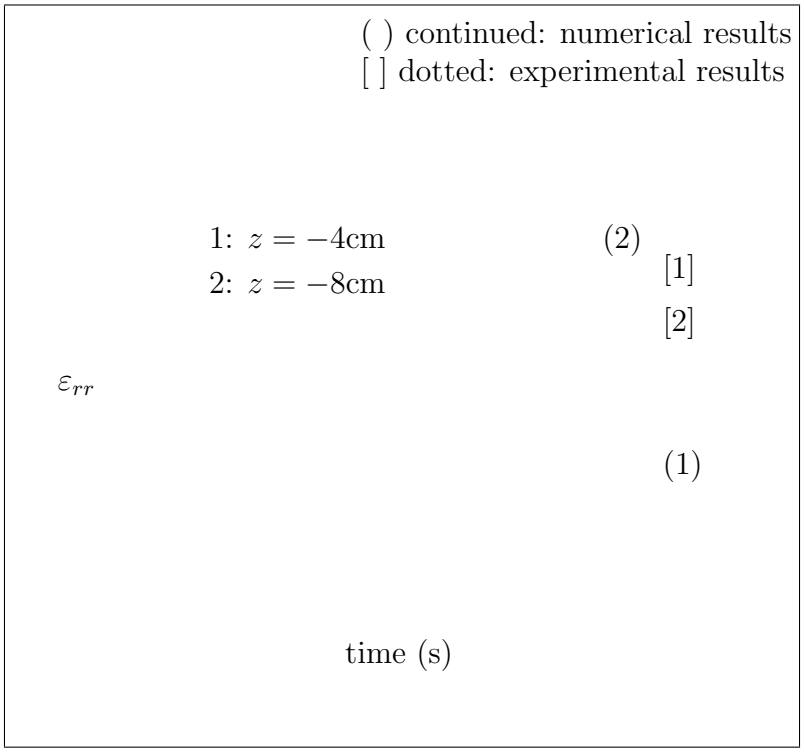

Figure 9: Radial strains ε_{rr} under the axis of loading

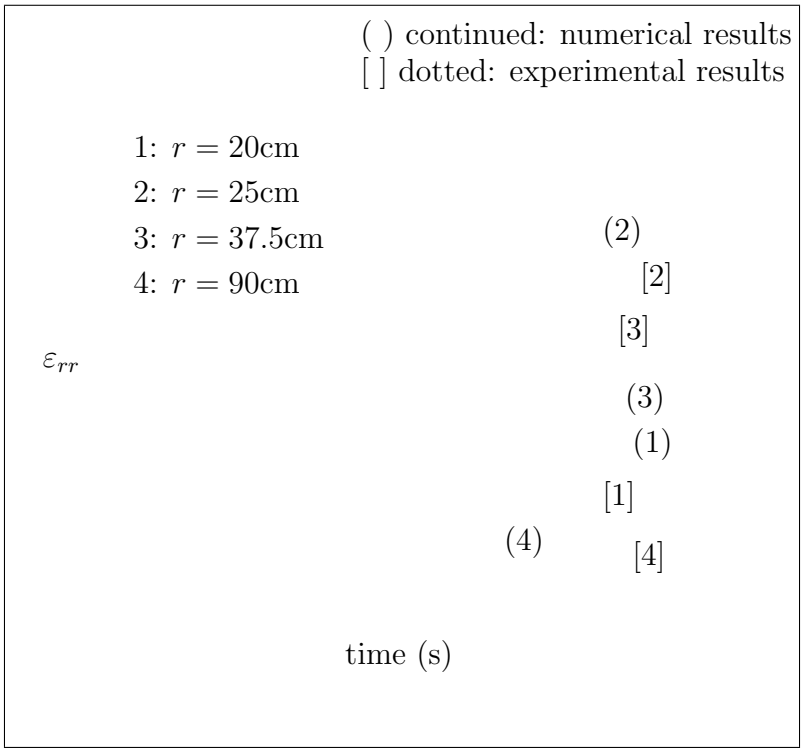

Figure 10: Radial strains ε_{rr} on the surface of the road

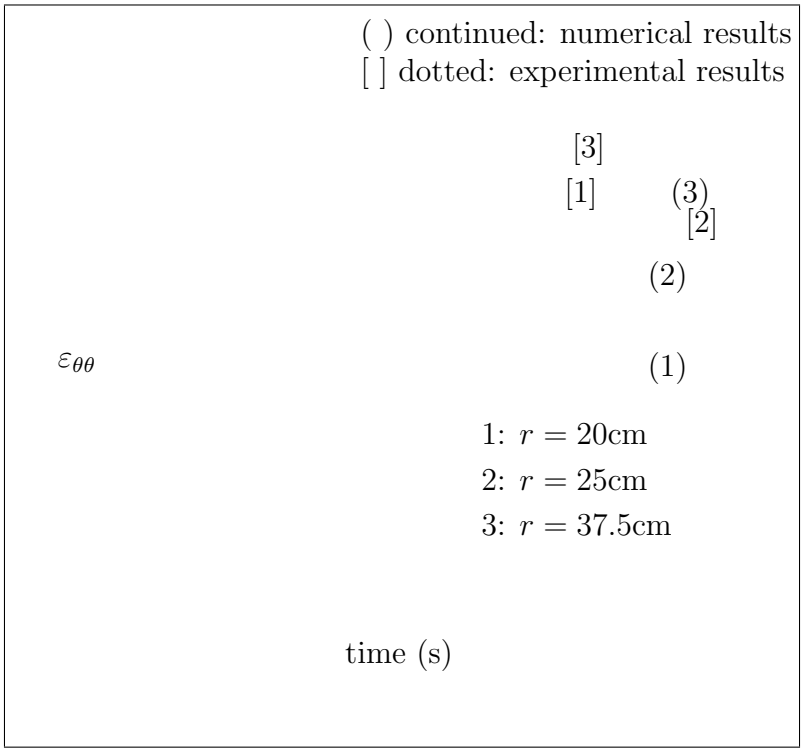

Figure 11: Orthoradial strains $\varepsilon_{\theta\theta}$ on the surface of the road

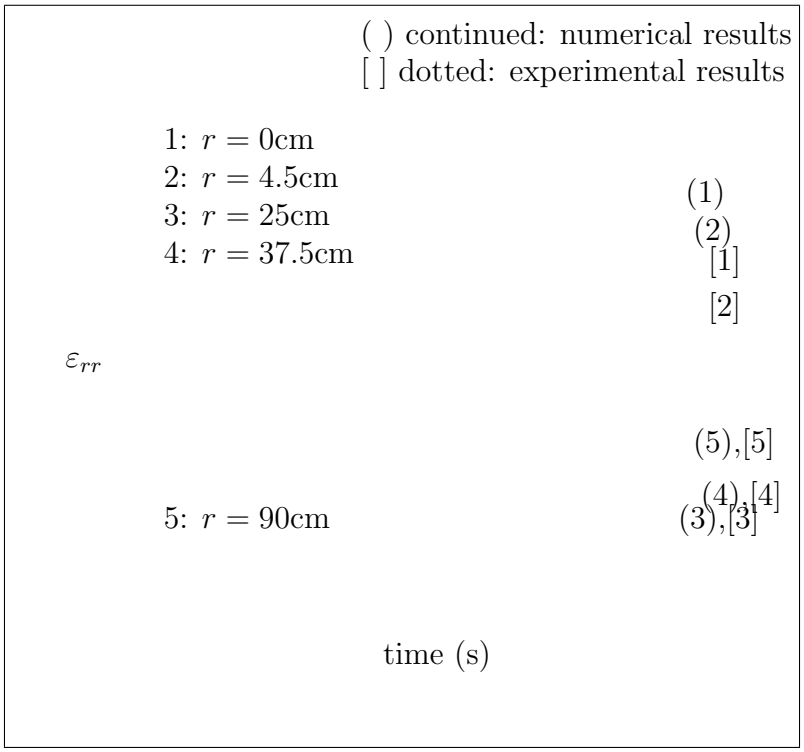

Figure 12: Radial strains ε_{rr} between bituminous concrete and sand

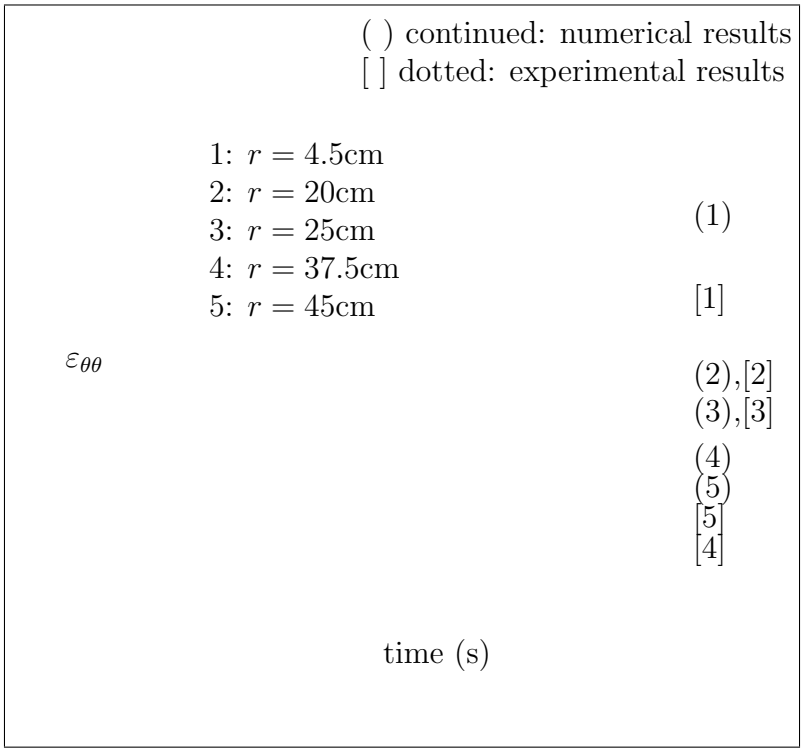

Figure 13: Orthoradial strains $\varepsilon_{\theta\theta}$ between bituminous concrete and sand